Electronic Supplementary Material (ESI) for Dalton Transactions.
This journal is © The Royal Society of Chemistry 2021

Supplementary Information

Chiral Wheel Anions of Copper(II)-Early Lanthanides(III) with High Optical-Limiting Properties

Xiongli Xu[#a], Yuan He[#b], Wei Meng[#c], Lu Yao [a], Liangliang Liu [a], Feng Xu*[a] and Chujun Zhao*[b]

Table of Content

Experimental Procedures

1. Materials and Methods:

All of the reactants were reagent grade and used as purchased. IR spectra were measured on PerkinElmer Spectrum 100 FT-IR spectrometer. Thermogravimetric analysis (TGA) measurements were carried out using a DSC/TG pan A1203 system in N_2 flow with a heating rate of 10 ℃ min^{-1}. Powder X-ray diffraction (PXRD) patterns were collected at room temperature on a Bruker D8 Advance. The EDS data were obtained using a MIRA3 LMA Oxford X MAX20. The solid-state and solution CD spectra were measured on MOS-500 Spectrometer. The solid UV-VIS-NIR were obtained using a UV-2600.The third-order NLO properties of the samples were evaluated using the open-aperture (OA) Z-scan technique. An 800 nm Ti: Sapphire amplifier system (Coherent, USA) was pumped to a femtosecond optical parametric amplifier (OPA) with a repetition rate of 1 kHz and a pulse duration of 35 fs. OPA outputs femtosecond laser, ~ 35 fs pulse duration and a repetition rate of 0.001 MHz. Use 200 mm focal length lens (N-BK7) as focusing lens. The power probes D1 and D2 (Newport, 918D-IR) are used to collect the input and output optical power of the sample. The spot size is measured by the knife-edge method, the spot radius at the focal point is 70um.

Synthesis of 1-10:

1: A mixture of $Cu(OAc)_2 \cdot H_2O$ (199 mg, 1 mmol), $La(NO_3)_3 \cdot 6H_2O$ (433 mg, 1 mmol) and L-(+)-tartaric acid (150 mg, 1 mmol) was dissolved in a potassium acetate/acetic acid buffer solution (pH 6.9, 2 M KOAc/HOAc, 10 mL). The mixture was stirred at room temperature for 12 h. Then the resulting blue solution was filtered and the filtrate was left undisturbed at ambient temperature. After several days, the blue square crystals were obtained by filtration. (The yield is 60% based on copper and 11% based on lanthanum) Anal. calcd for $C_{80}H_{190}Cu_{22}K_{16}La_4O_{179}$: C 14.57, H 2.90. Found: C 14.90, H 2.44. In order to improve the yield of rare earth elements, a series of synthetic experiments with larger ratio of copper to lanthanide were carried out. The results show that the ratio of Cu/La 2:1 (yield of 22% based on La), can still leads to the crystallization of **1** while the ratio larger than 2:1 no longer gives the crystals of **1**.

2 was prepared in a similar fashion to **1** except that D-(-)-tartaric acid was used instead of L-(+)-tartaric acid (yield 60% based on copper and 11% based on lanthanoids, 22% based on La when the ratio of Cu/La is 2:1). Anal. calcd for $C_{80}H_{216}Cu_{22}K_{16}La_4O_{192}$: C 14.09, H 3.04. Found: C 13.97, H 2.36.

3: A mixture of $Cu(OAc)_2 \cdot H_2O$ (199 mg, 1 mmol), $Ce(NO_3)_3 \cdot 6H_2O$ (434 mg, 1 mmol) and L-(+)-tartaric acid (150 mg, 1 mmol) was dissolved in a potassium acetate/acetic acid buffer solution (pH 6.9, 2 M KOAc/HOAc, 10 mL). The mixture was stirred at room temperature for 12 h. Then the resulting blue solution was filtered and the filtrate

was left undisturbed at ambient temperature. After several days, the blue square crystals were obtained by filtration. The yield is 60% based on copper and 11% based on cerium, 22% based on Ce when the ratio of Cu/Ce is 2:1) Anal. calcd for $C_{80}H_{220}Cu_{22}K_{16}Ce_4O_{194}$: C 13.94, H 3.51. Found: C 14.04, H 3.13.

4 was prepared in a similar fashion to **3** except that D-(-)-tartaric acid was used instead of L-(+)-tartaric acid (yield 60% based on copper and 11% based on cerium, 22% based on Ce when the ratio of Cu/Ce is 2:1) Anal. calcd for $C_{80}H_{220}Cu_{22}K_{16}Ce_4O_{194}$:C 13.99, H 3.23. Found: C 13.87, H 2.97.

5: A mixture of $Cu(OAc)_2 \cdot H_2O$ (199 mg, 1 mmol), $Pr(NO_3)_3 \cdot 6H_2O$ (435 mg, 1 mmol) and L-(+)-tartaric acid (150 mg, 1 mmol) was dissolved in a potassium acetate/acetic acid buffer solution (pH 6.9, 2 M KOAc/HOAc, 10 mL). The mixture was stirred at room temperature for 12 h. Then the resulting blue solution was filtered and the filtrate was left undisturbed at ambient temperature. After several days, the blue square crystals were obtained by filtration. (The yield is 50% based on copper and 9% based on praseodymium, 18% based on Pr when the ratio of Cu/Pr is 2:1) Anal. calcd for $C_{80}H_{180}Cu_{22}K_{16}Pr_4O_{174}$: C 14.79, H 2.76. Found: C 14.75, H 2.67.

6 was prepared in a similar fashion to **5** except that D-(-)-tartaric acid was used instead of L-(+)-tartaric acid (yield 60% based on copper and 9.2% based on praseodymium, 18.4% based on Pr when the ratio of Cu/Pr is 2:1). Anal. calcd for $C_{80}H_{180}Cu_{22}K_{16}Pr_4O_{174}$: C 14.75, H 2.79. Found: C 14.67, H 2.69.

7: A mixture of $Cu(OAc)_2 \cdot H_2O$ (199 mg, 1 mmol), $Nd(NO_3)_3 \cdot 6H_2O$ (438 mg, 1 mmol) and L-(+)-tartaric acid (150 mg, 1 mmol) was dissolved in a potassium acetate/acetic acid buffer solution (pH 6.9, 2 M KOAc/HOAc, 10 mL). The mixture was stirred at room temperature for 12 h. Then the resulting blue solution was filtered and the filtrate was left undisturbed at ambient temperature. After several days, the blue square crystals were obtained by filtration. (The yield is 60% based on copper and 11% based on neodymium, 22% based on Nd when the ratio of Cu/Nd is 2:1) Anal. calcd for $C_{80}H_{168}Cu_{22}K_{16}Nd_4O_{168}$: C 15.00, H 2.64. Found: C 14.47, H 1.99.

8 was prepared in a similar fashion to **7** except that D-(-)-tartaric acid was used instead of L-(+)-tartaric acid (yield 60% based on copper and 11% based on neodymium, 22% based on Nd when the ratio of Cu/Nd is 2:1). Anal. calcd for $C_{80}H_{186}Cu_{22}K_{16}Nd_4O_{177}$: C14.63, H 2.85. Found: C 14.53, H 2.66.

9: A mixture of $Cu(OAc)_2 \cdot H_2O$ (199 mg, 1 mmol), $SmCl_3 \cdot 6H_2O$ (365 mg, 1 mmol) and L-(+)-tartaric acid (150 mg, 1 mmol) was dissolved in a potassium acetate/acetic acid buffer solution (pH 6.9, 2 M KOAc/HOAc, 10 mL).The mixture was stirred at room temperature for 12 h. Then the resulting blue solution was filtered and the filtrate was left undisturbed at ambient temperature. After several days, the blue square crystals were obtained by filtration. (The yield is 40% based on copper and 7% based on samarium, 14% based on Sm when the ratio of Cu/Sm is 2:1) Anal. calcd for $C_{80}H_{230}Cu_{22}K_{16}Sm_4O_{199}$: C 13.69, H 3.28 Found: C 13.39, H:3.12.

10 was prepared in a similar fashion to **9** except that D-(-)-tartaric acid was used instead

of L-(+)-tartaric acid (The yield is 40% based on copper and 7% based on samarium, 11% based on Sm when the ratio of Cu/Sm is 2:1) Anal. calcd for $C_{80}H_{230}Cu_{22}K_{16}Sm_4O_{199}$: C 13.69, H 3.28. Found: C 13.54, H 3.14.

2. Synthesis of the third-order NLO test films

Poly (methyl methacrylate) (PMMA) (0.52 g)and L-$Cu_{22}Ln_4$ (Ln= La, Ce, Pr, Nd, and Sm)(0.002g) were mixed and dispersed in 10 ml trichloromethane at concentration ~0.2 g/L. The mixture is thoroughly blended at room temperature with a magnetic stirrer and ultrasonic agitation. The mixture was transferred to petri dishes of the same size and placed in an oven at 40℃ until the solvent was completely volatilized. The preparation process of pure PMMA thin film is the same as above, without adding L-$Cu_{22}Ln_4$ (Ln= La, Ce, Pr, Nd, and Sm).

3. Z-scan measurements

The measured Z-scan curves were fitted using the following expressions:

$$T(Z,S=1)=\frac{1}{\sqrt{\pi}q_0(Z,0)}\int_{-\infty}^{+\infty} ln\left[1+q_0(Z,0)e^{-r^2}\right]dr \quad (1)$$

$$q_0(Z,0)=\beta I_0 L_{eff} \quad (2)$$

$$L_{eff}=\frac{1-e^{-\alpha l}}{\alpha} \quad (3)$$

Where, I_0 is the on-axis peak intensity at the focus (Z = 0), L_{eff} is the effective thickness of the sample, α_0 is the linear absorption coefficient, l is the sample thickness, z is the Z-scan displacement.

The relationship of the sample transmission and input fluence can be plotted from the open-aperture Z-scan curve[1, 2]. From the input laser pulse energy E_{in} and beam radius $\omega(z)$, the light fluence $F_{in}(z)$ at any position can be obtained. $F_{in}(z)$ is defined as:

$$F_{in}(z)=\frac{4\sqrt{ln2E_{in}}}{\pi^{\frac{3}{2}}\omega(z)^2}$$

Where ω(z) is defined as:

$$\omega(z)=\frac{\omega_0}{[1+\left(\frac{z}{z_0}\right)^2]^{\frac{1}{2}}}$$

$z_0=\frac{\pi{\omega_0}^2}{2}$ is the Rayleigh range. $k=\frac{2\pi}{\lambda}$, ω_0 is the beam radius at the focus, and I_0 is the input peak intensity at the focus. The calculated value of effective path length

(800 nm) is found to be much less than Rayleigh range (z_0), satisfying the thin film approximation $L_{eff} \ll z_0$.

4. Crystallography

Data collection was performed at 150 K on a BRUKER D8 QUEST with graphite-monochromated $Mo_{K\alpha}$ radiation (λ = 0.71073Å). Suitable crystals were affixed to the end of a glass fiber using silicone grease and transferred to the goniostat. The structures of 7 compounds were solved by the direct method and refined by the full-matrix least-squares method on F^2 using the *SHELXL-2016/6* (Sheldrick, 2016) software package. Crystallographic data and structural refinements for compounds **1-3, 5-7** are summarized in Table S1 and Table S2. More details on the crystallographic studies as well as atomic displacement parameters are given in the CIF files. All carbon-bonded hydrogen atoms were placed in geometrically calculated positions; hydrogen atoms in water molecules were not assigned or directly included in the molecular formula. In all structures, the clusters and their associated ligands were modeled and refined. A few solvent areas in **5-7** were disordered so badly that it could not be modeled even with restraints. Consequently, SQUEEZE (from PLATON) was used to calculate the void space, the electron count and to produce new HKL files for further refinements. According to the SQUEEZE results, the number of solvent molecules H_2O masked were assessed for compound **5-7**. Details of the masked entities per unit cell are summarized as below. Compound **5**: $90H_2O$ (2836 $Å^3$ void and 911 electrons count from SQUEEZE); **6**: $78H_2O$ (2824 $Å^3$ and 782 electrons); **7**: $40H_2O$ (2814 $Å^3$ and 407 electrons). SQUEEZE procedure improved the quality of all structures applied.

Table S1. Crystal data and structure refinement for complexes **1**-**3**.

Compounds	**1**	**2**	**3**
Empirical formula	$C_{20}H_{14}Cu_{5.48}K_{3.35}La_{1.02}O_{35.18}$	$C_{10}H_7Cu_{2.74}K_{1.68}La_{0.51}O_{17.62}$	$C_{40}H_{28}Cu_{10.98}K_{6.70}Ce_{2.02}O_{70.58}$
fw	1438.15	719.39	2880.76
cryst syst	Tetragonal	Tetragonal	Tetragonal
space group	I 4 2 2	I 4 2 2	I 4 2 2
a [Å]	23.119(9)	23.067(3)	23.212(3)
b [Å]	23.119(9)	23.067(3)	23.212(3)
c [Å]	17.971(8)	17.923(3)	18.090(3)
α [deg]	90	90	90
β [deg]	90	90	90
γ [deg]	90	90	90
V [$Å^3$]	9605(9)	9537(3)	9747(3)
Z	8	16	4
Dcalcd [g/cm^{-3}]	1.989	2.004	1.963
μ [mm^{-1}]	3.647	3.673	3.651
F(000)	5272	5272	5280
Flack parameter	-0.02(4)	0.011(7)	0.09(4)
goodness-of-fit on F^2	1.069	1.059	1.062
R indices (all data)	R1 =0.0428 (3743) wR2 = 0.1293 (4096)	R1 = 0.0394 (4158) wR2= 0.1189 (4376)	R1 =0.0581(5345) wR2 =0.1624(6032)

Table S2. Crystal data and structure refinement for complexes **5**-**7**.

Compounds	**5**	**6**	**7**
Empirical formula	$C_{60}H_{42}$ $Cu_{16.50}K_{6.75}Pr_3O_{100.12}$	$C_{20}H_{14}Cu_{5.50}K_{2.25}PrO_{33.38}$	$C_{80}H_{52}Cu_{22}K_9Nd_4O_{133}$
fw	4100.00	1366.67	5467.95
cryst syst	Cubic	Cubic	Cubic
space group	I 4 3 2	I 4 3 2	I 4 3 2
a [Å]	39.543(8)	39.5746(14)	39.498(2)
b [Å]	39.543(8)	39.5746(14)	39.498(2)
c [Å]	39.543(8)	39.5746(14)	39.498(2)
α [deg]	90	90	90
β [deg]	90	90	90
γ [deg]	90	90	90
V [Å ^{3}]	61830(38)	61890(7)	61621(9)
Z	16	48	12
Dcalcd [g/cm^{-3}]	1.762	1.758	1.768
μ [mm^{-1}]	3.422	3.413	3.495
F(000)	31788.0	31788.0	31740
Flack parameter	0.02(3)	0.05(3)	0.01(2)
goodness-of-fit on F^2	1.059	1.068	1.086
R indices (all data)	R1 = 0.0527(8747) wR2 = 0.1523(10122)	R1 =0.0600(9533) wR2 =0.1735(10059)	R1 =0.0424(9707) wR2 =0.1213(10075)

Section S2: Supplementary Structural Fig.s

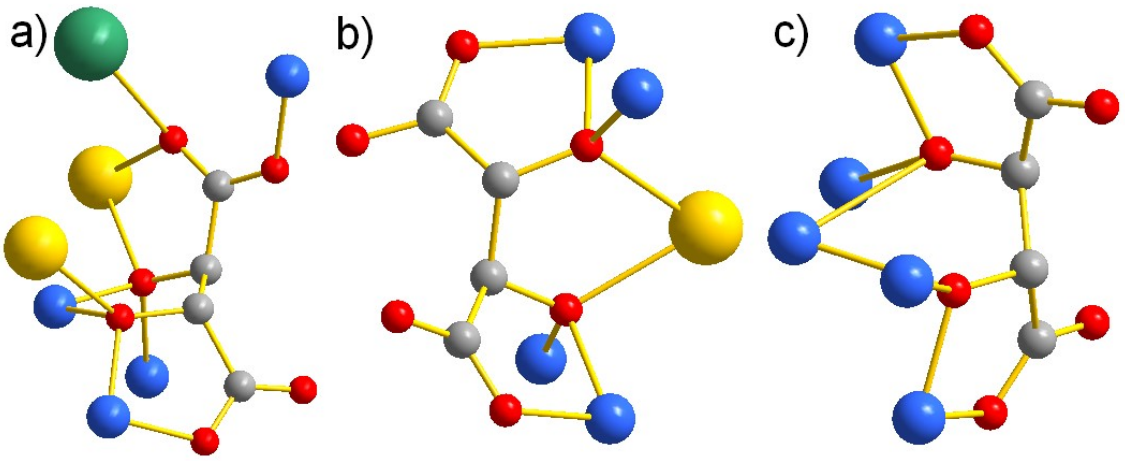

Fig. S1. Schematic view of three coordination modes of the tartrate ligands in **5**. Color code: Cu blue, Pr yellow, K green, O red, C gray, hydrogen atoms omitted for clarity.

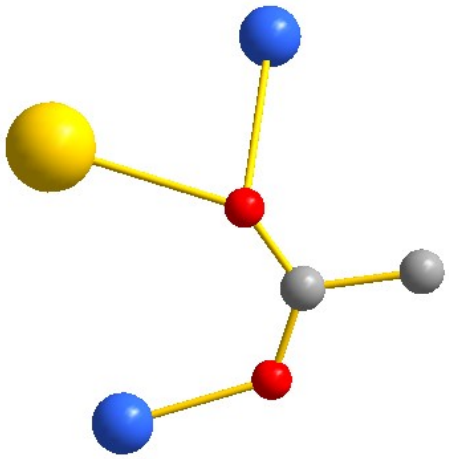

Fig. S2. Schematic view of coordination mode of the acetate ligands in **5**. Color code: Cu blue, Pr yellow, O red, C gray, hydrogen atoms omitted for clarity.

Section S3: Supplementary Physical Characterization

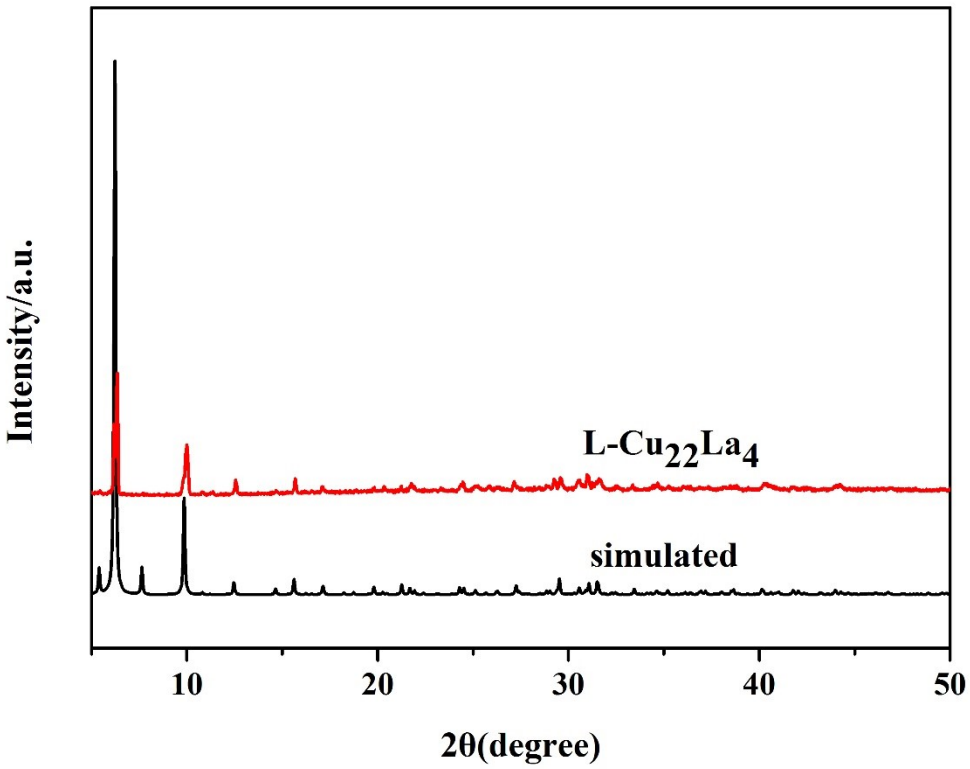

Fig. S3. Simulated and observed powder X-ray diffraction (PXRD) of **1**.

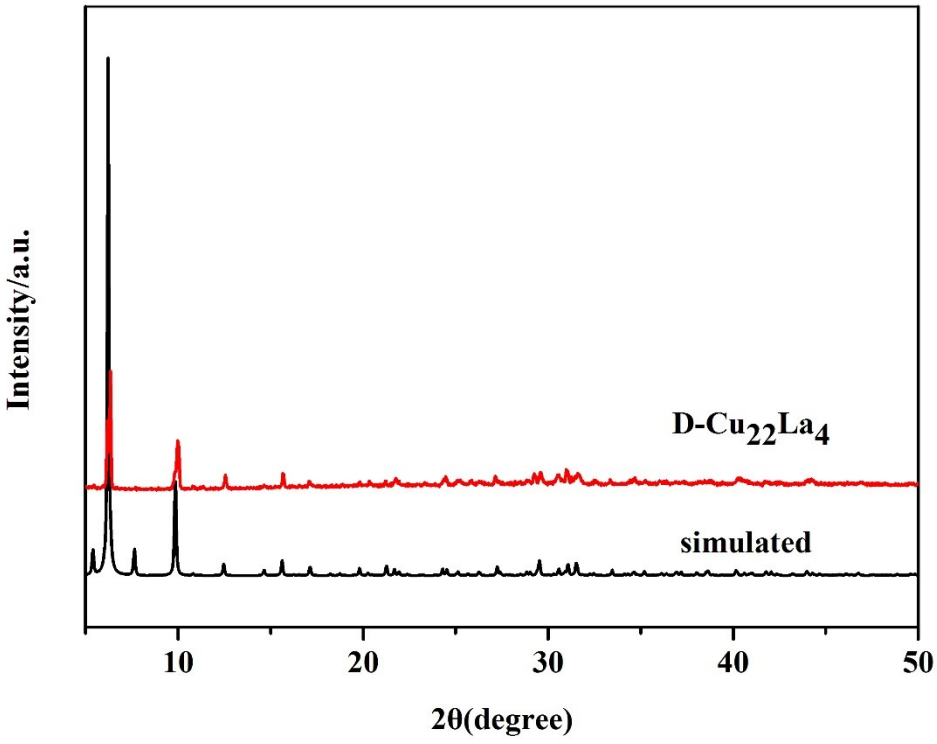

Fig. S4. Simulated and observed powder X-ray diffraction (PXRD) of **2**.

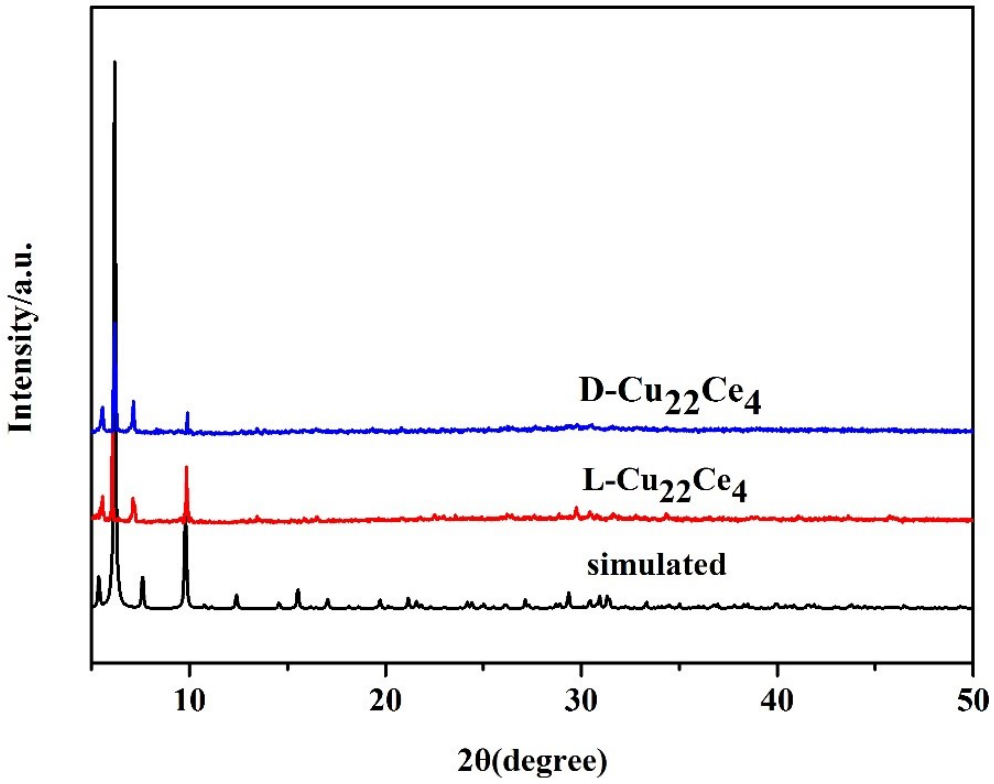

Fig. S5. Simulated and observed powder X-ray diffraction (PXRD) of **3** and **4**.

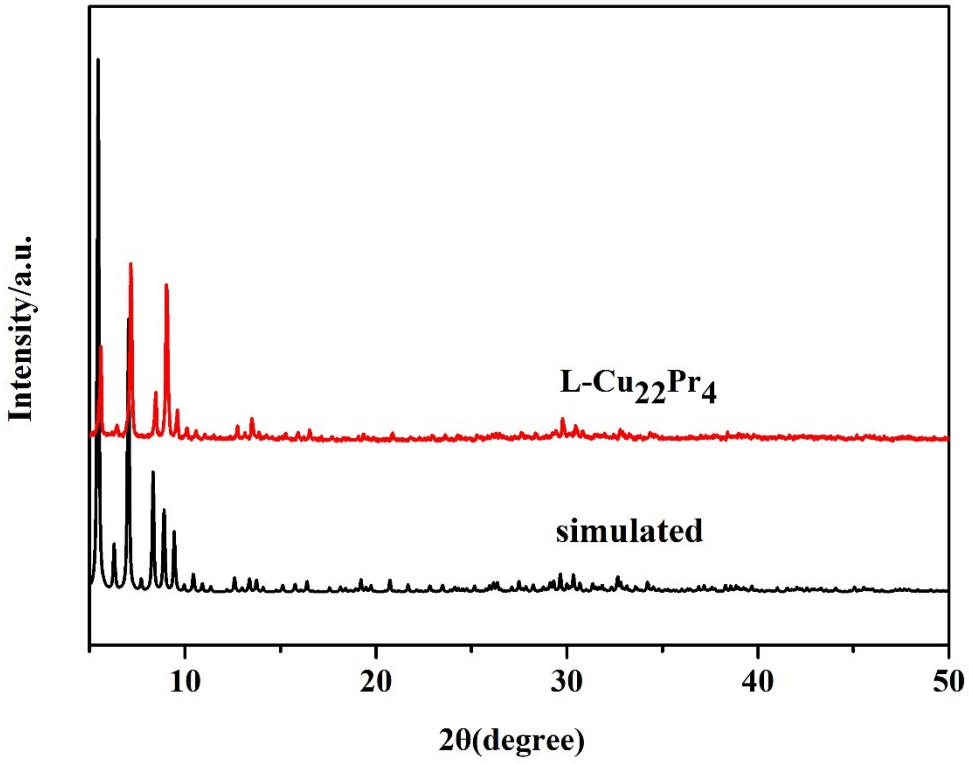

Fig. S6. Simulated and observed powder X-ray diffraction (PXRD) of **5**.

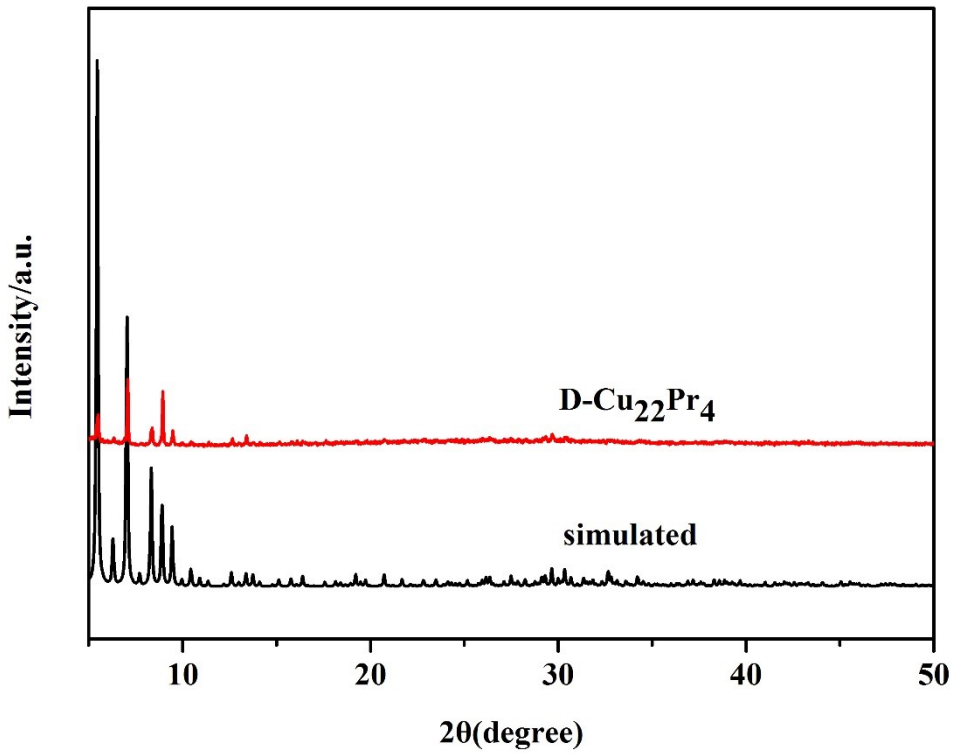

Fig. S7. Simulated and observed powder X-ray diffraction (PXRD) of **6**

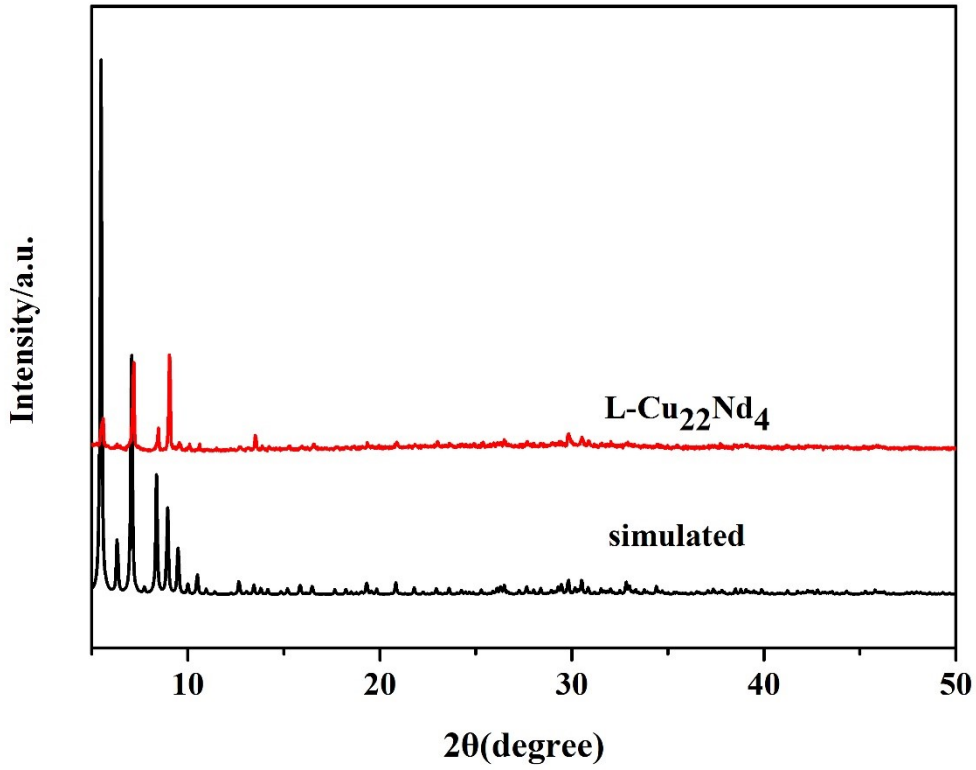

Fig. S8. Simulated and observed powder X-ray diffraction (PXRD) of **7**.

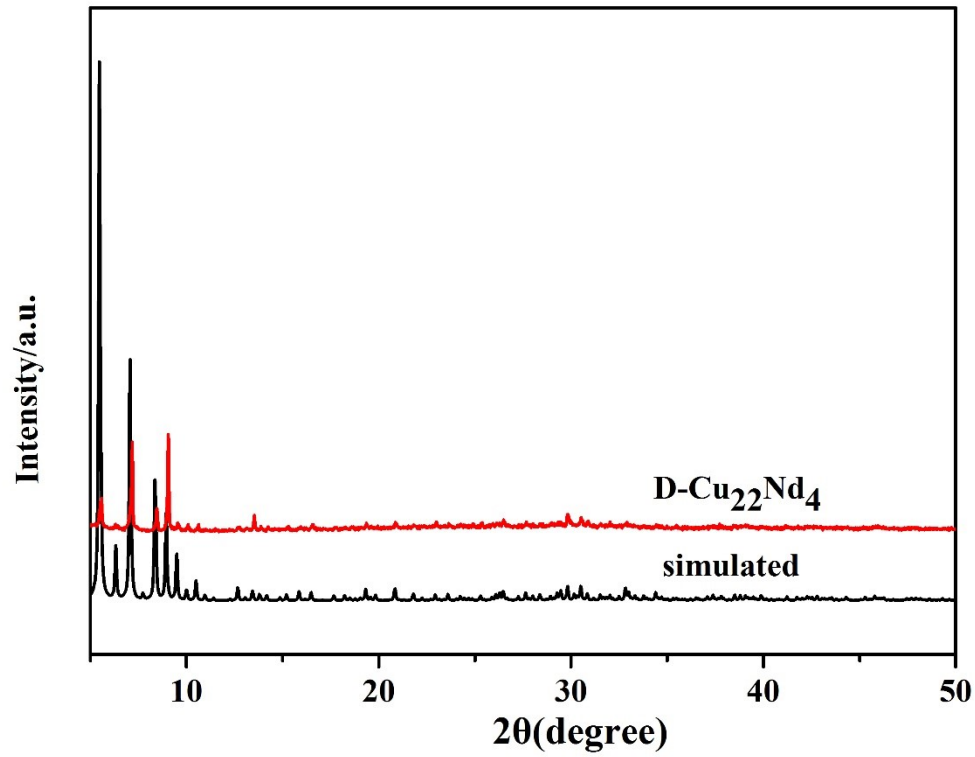

Fig. S9. Simulated and observed powder X-ray diffraction (PXRD) of **8**.

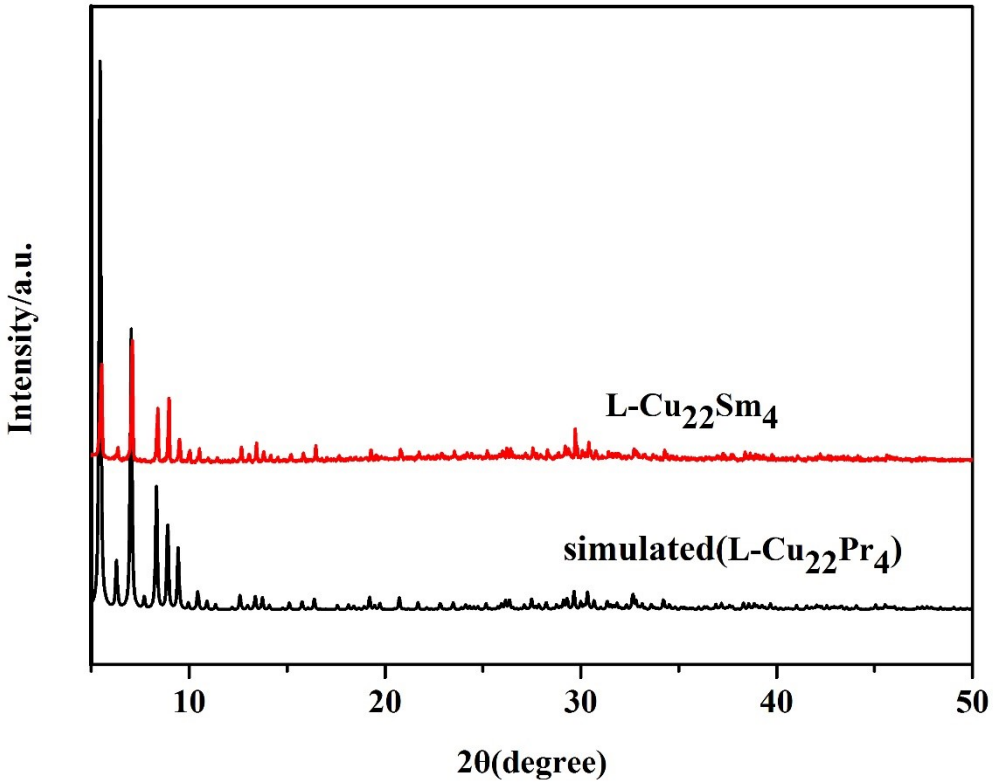

Fig. S10 Simulated and observed powder X-ray diffraction (PXRD) of **9**.

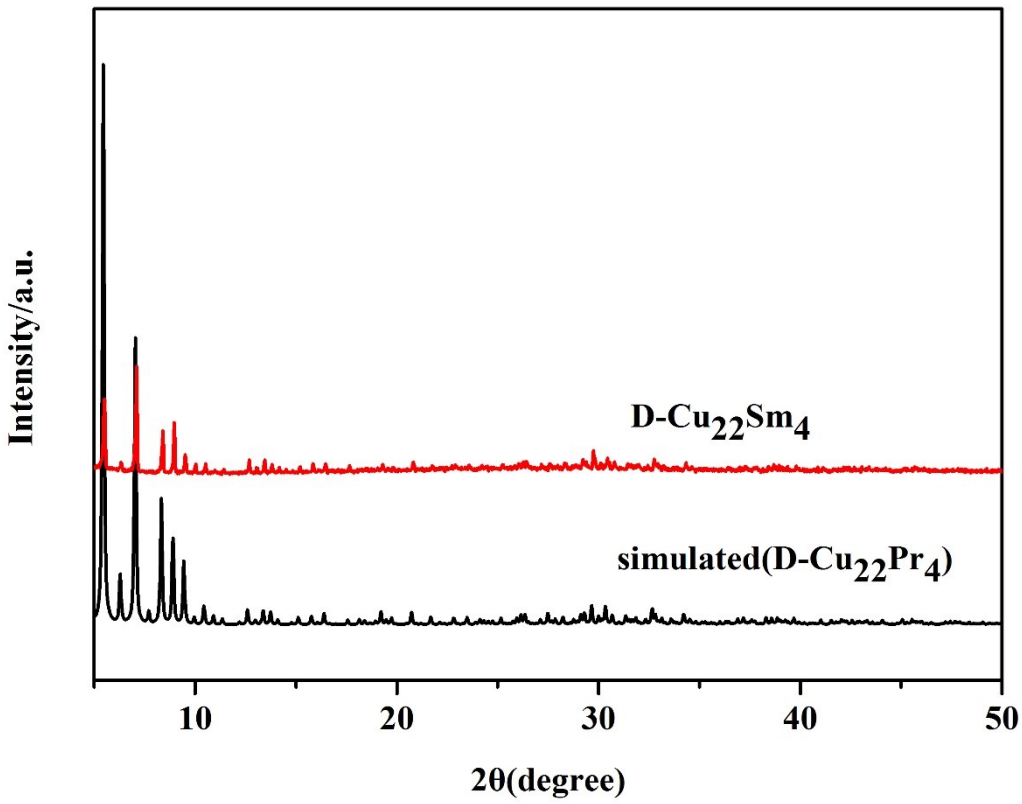

Fig. S11. Simulated and observed powder X-ray diffraction (PXRD) of **10**.

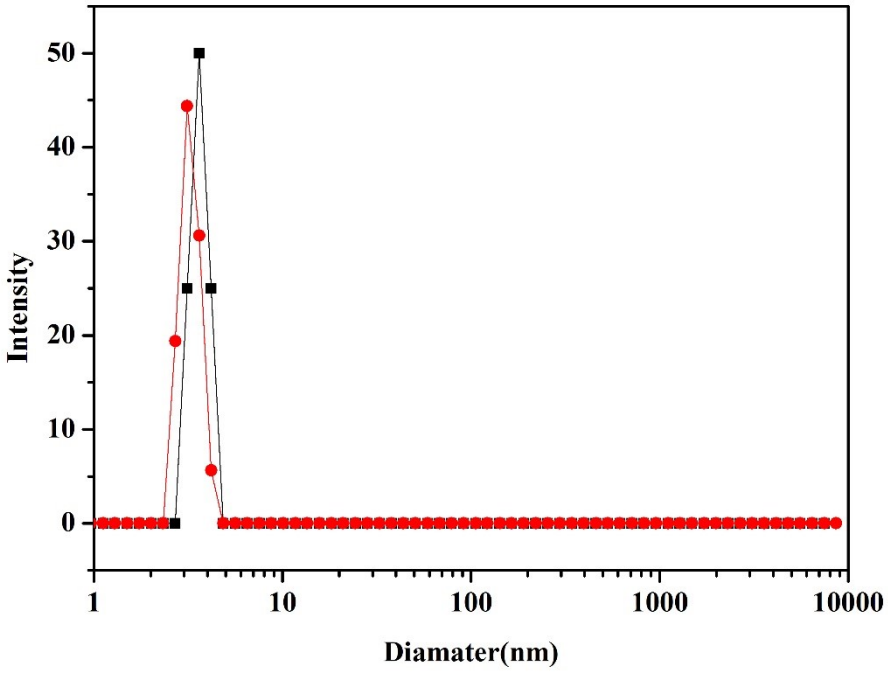

Fig. S12. Size distribution by number of nanoparticles for 0.1 mM **1** aqueous solution (black, crystals sonicated for 6 hours); Size distribution by number of nanoparticles for 0.1 mM **1** aqueous solution after 24 hours (red).

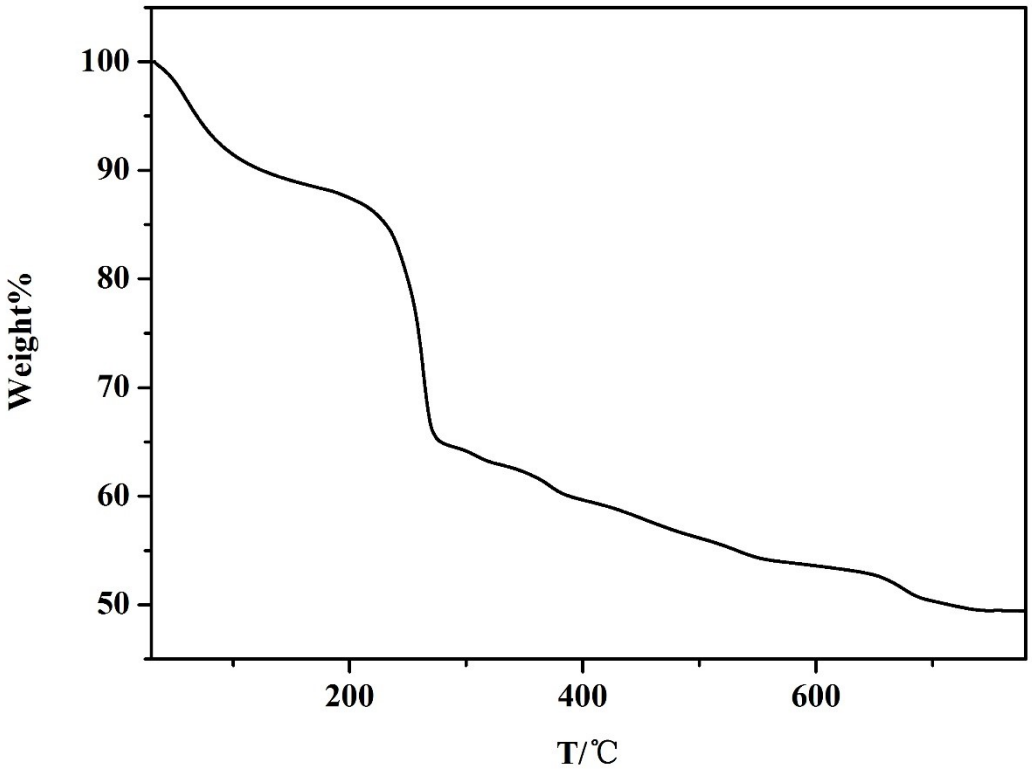

Fig. S13 TGA of **1** in the N_2 flow.

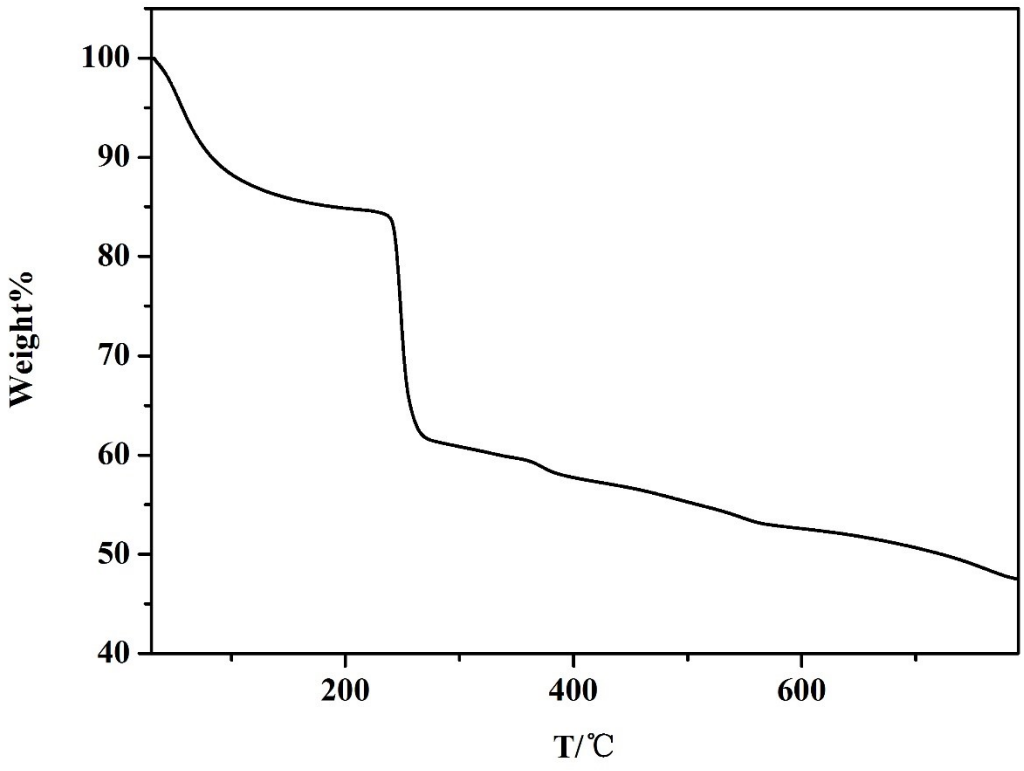

Fig. S14. TGA of **3** in the N_2 flow.

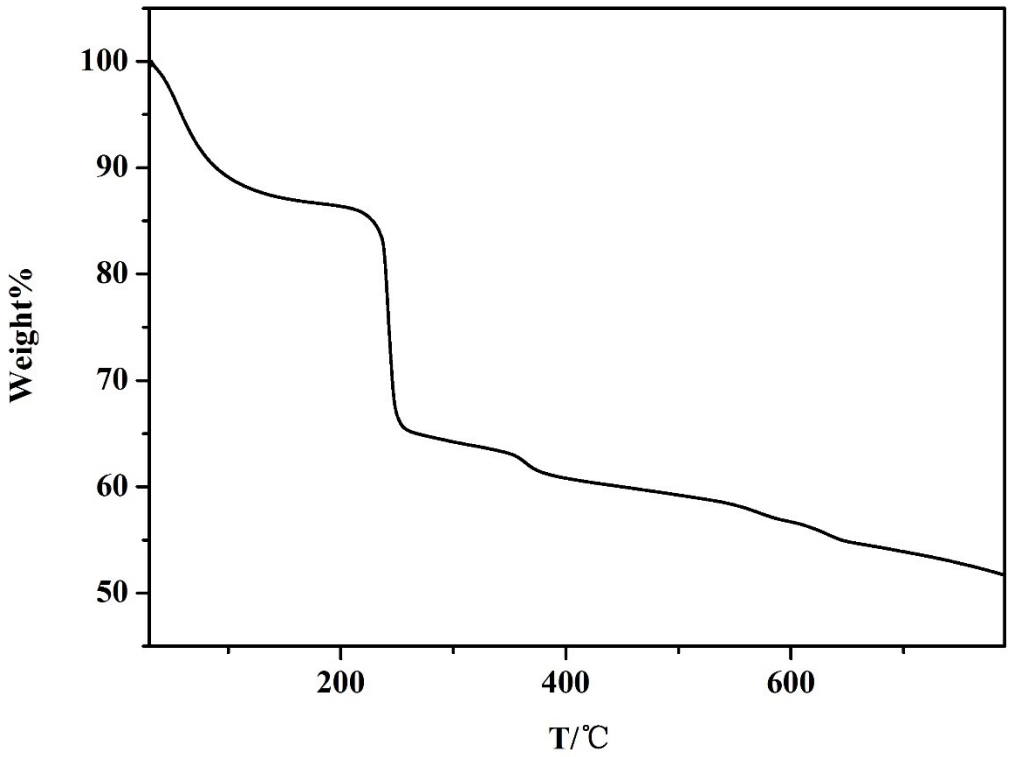

Fig. S15. TGA of **5** in the N_2 flow.

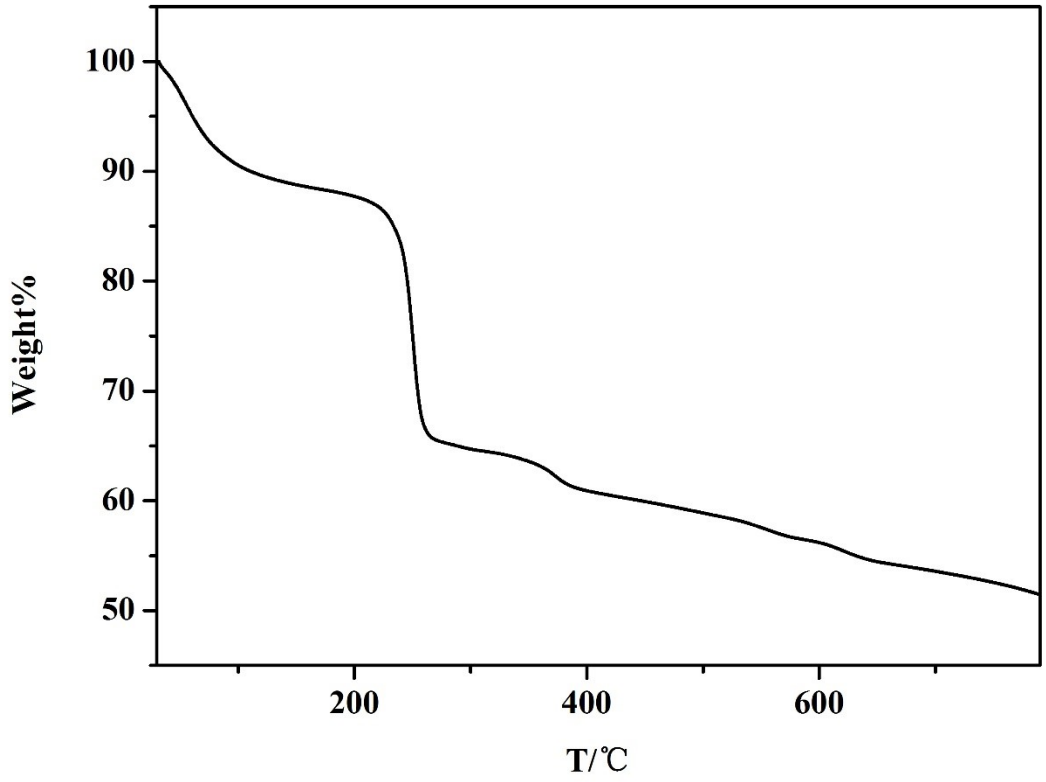

Fig. S16. TGA of **7** in the N_2 flow.

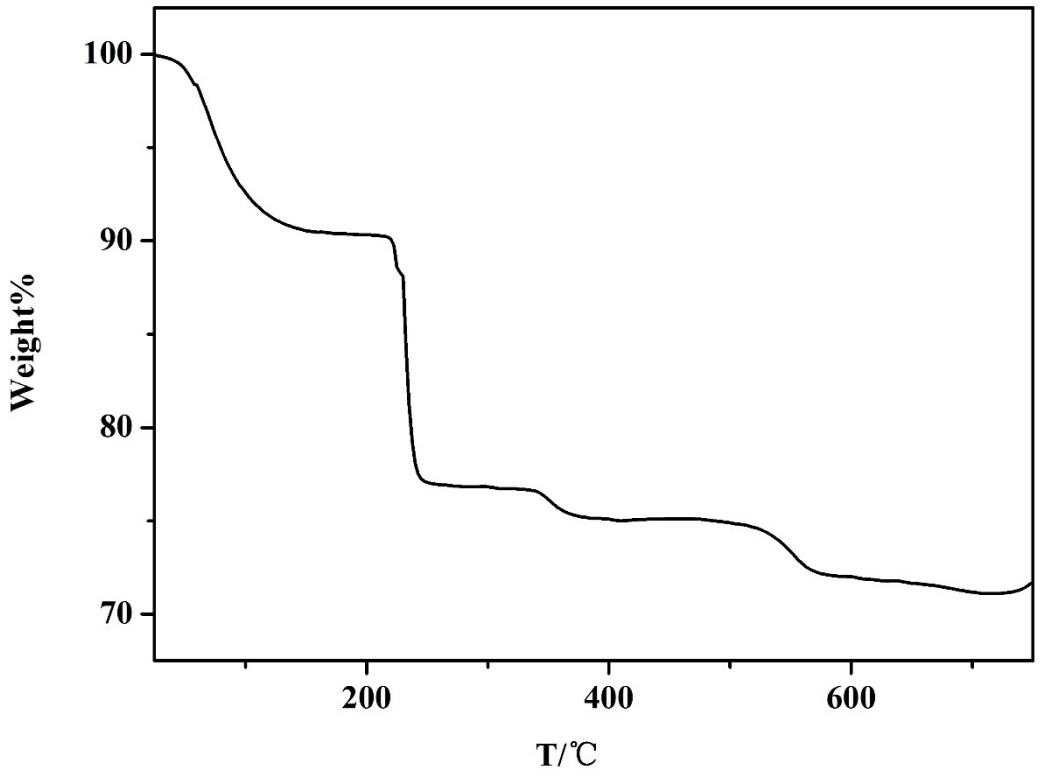

Fig. S17. TGA of **9** in the N_2 flow.

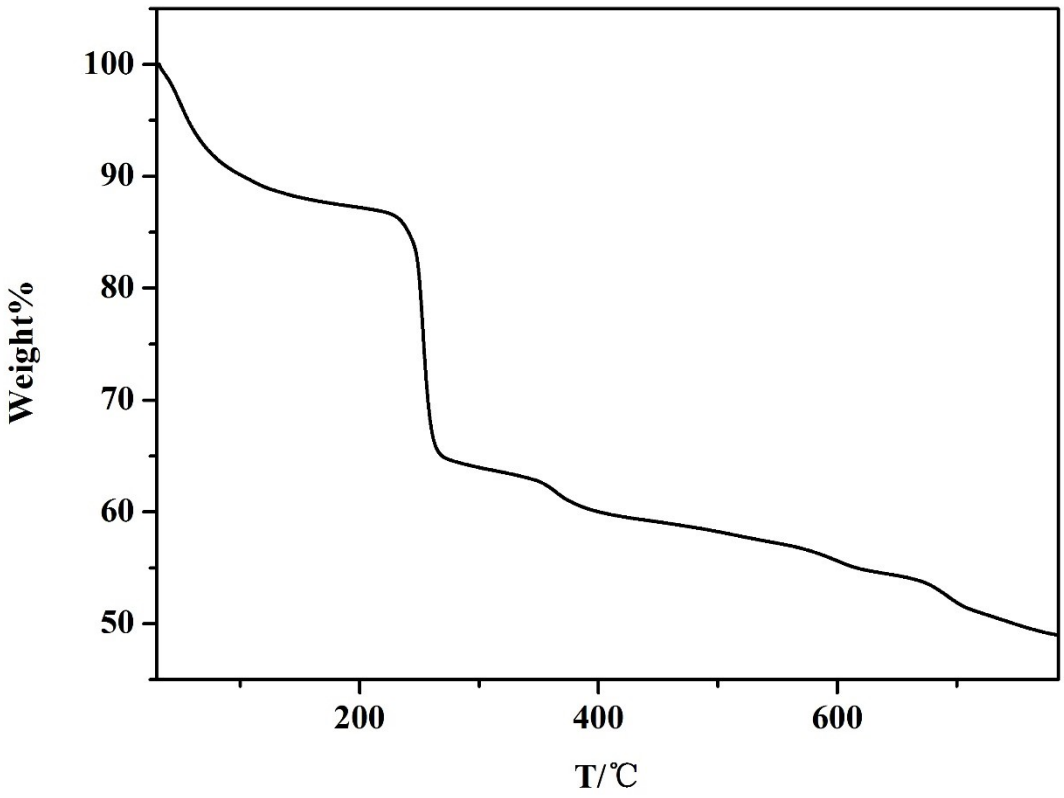

Fig. S18. TGA of **2** in the N_2 flow.

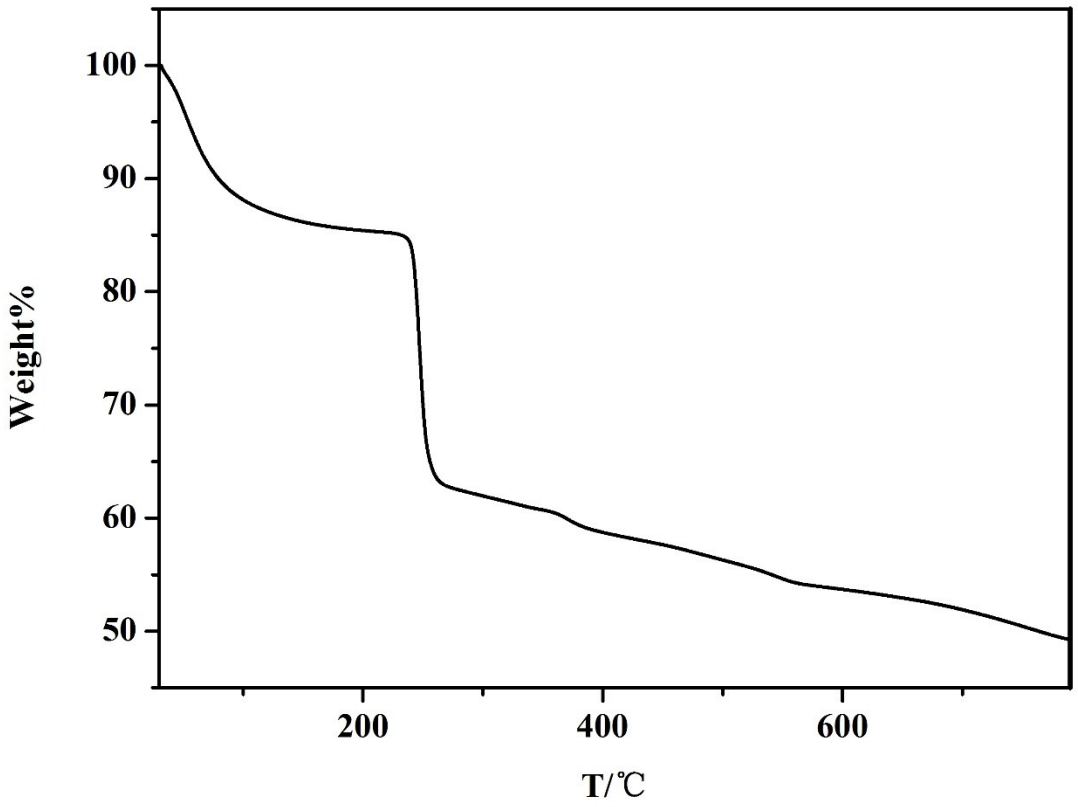

Fig. S19. TGA of **4** in the N_2 flow.

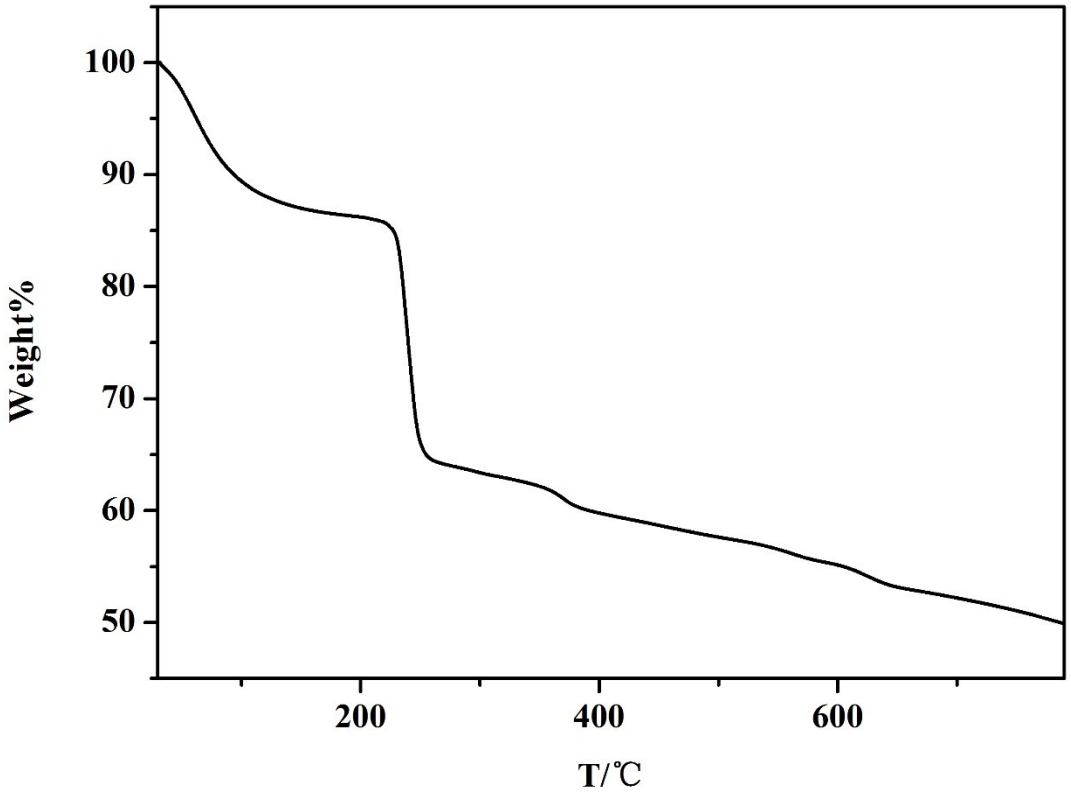

Fig. S20. TGA of **6** in the N_2 flow.

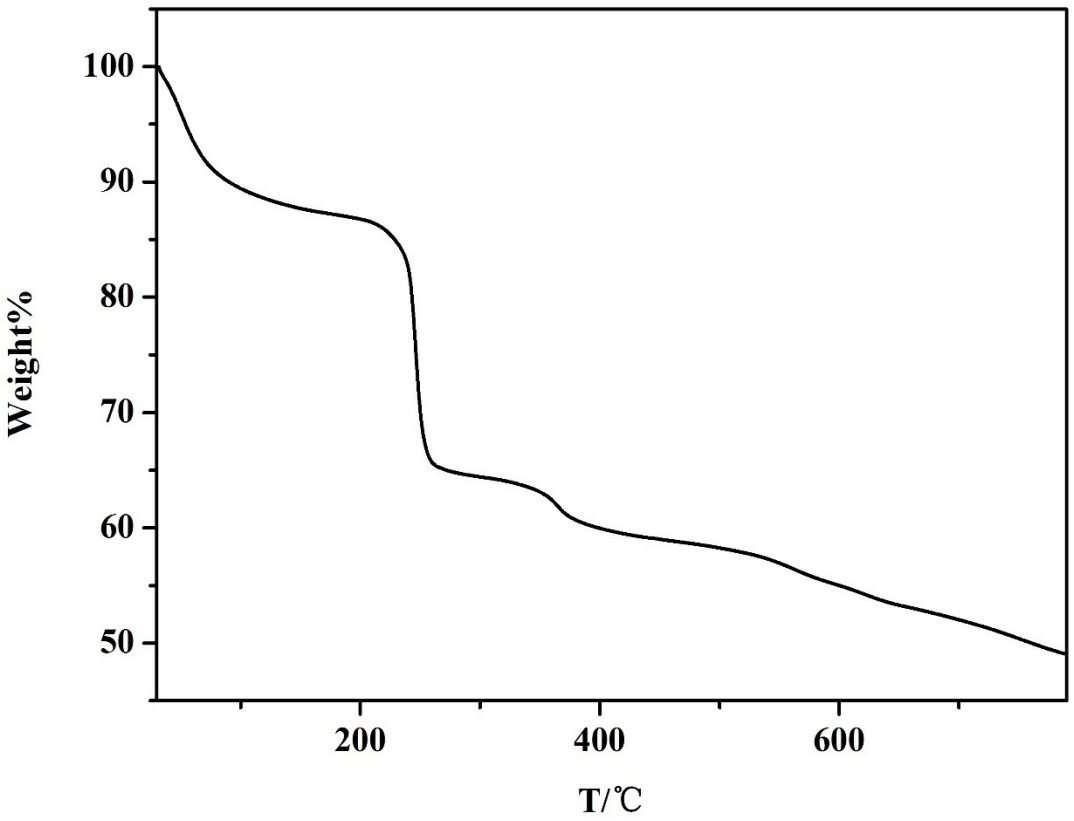

Fig. S21. TGA of **8** in the N_2 flow.

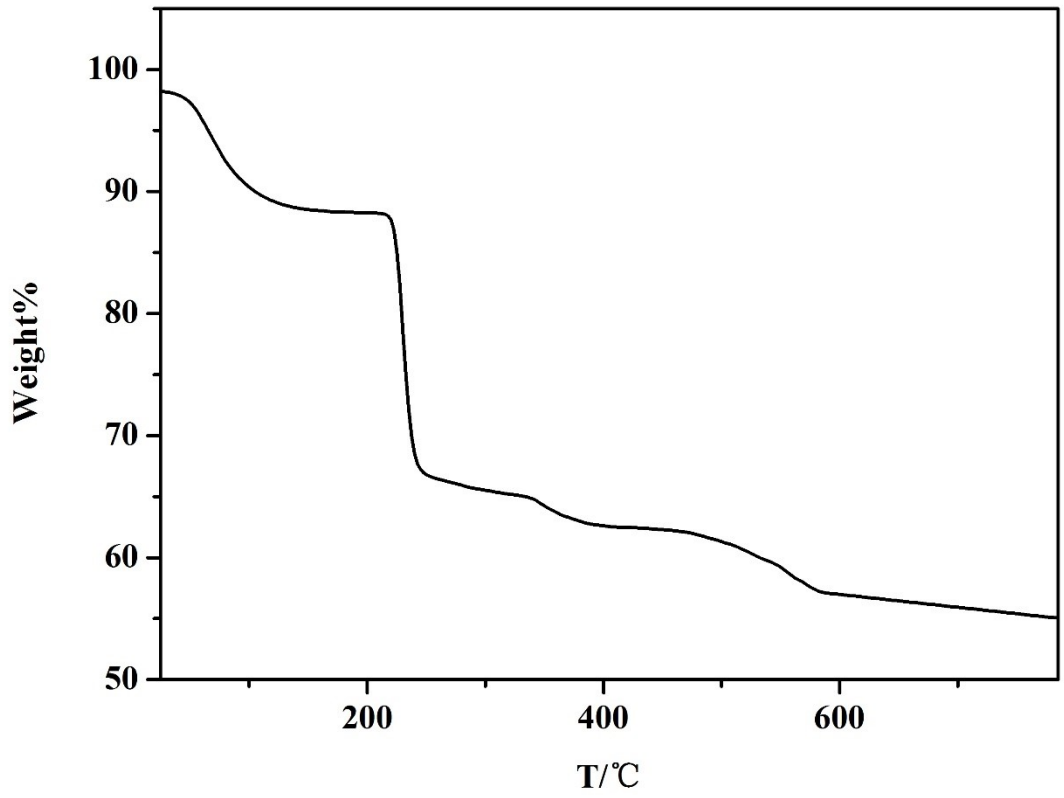

Fig. S22. TGA of **10** in the N_2 flow.

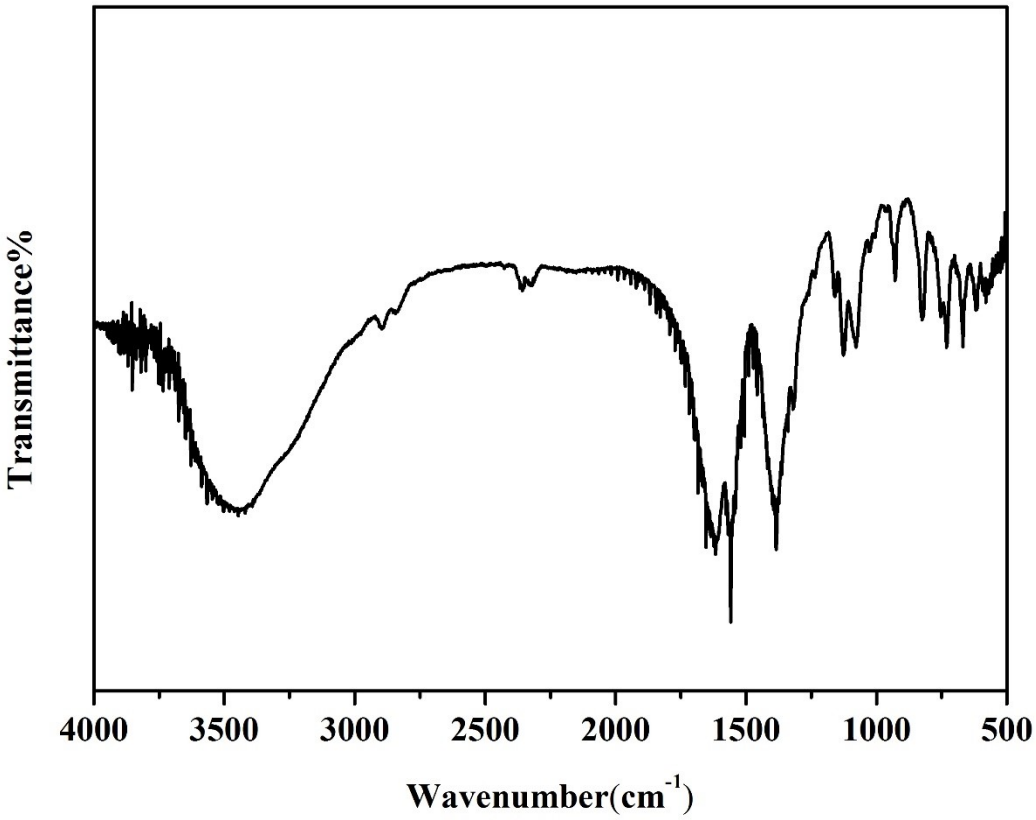

Fig. S24. IR spectrum of **1** (measured in KBr pellets).

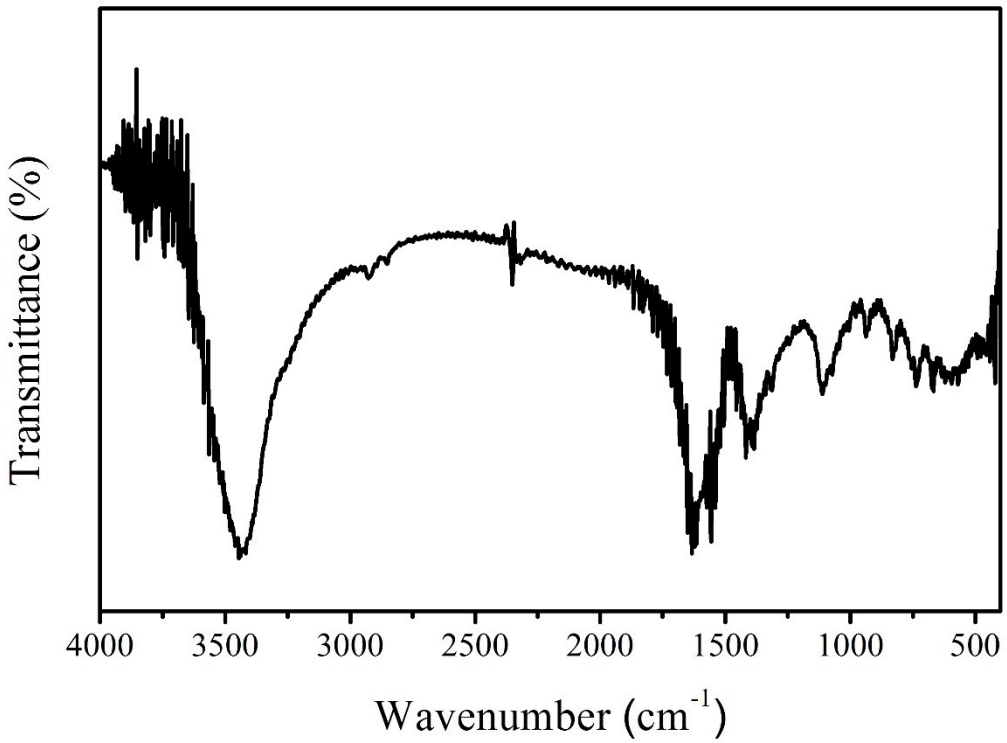

Fig. S25. IR spectrum of **3** (measured in KBr pellets).

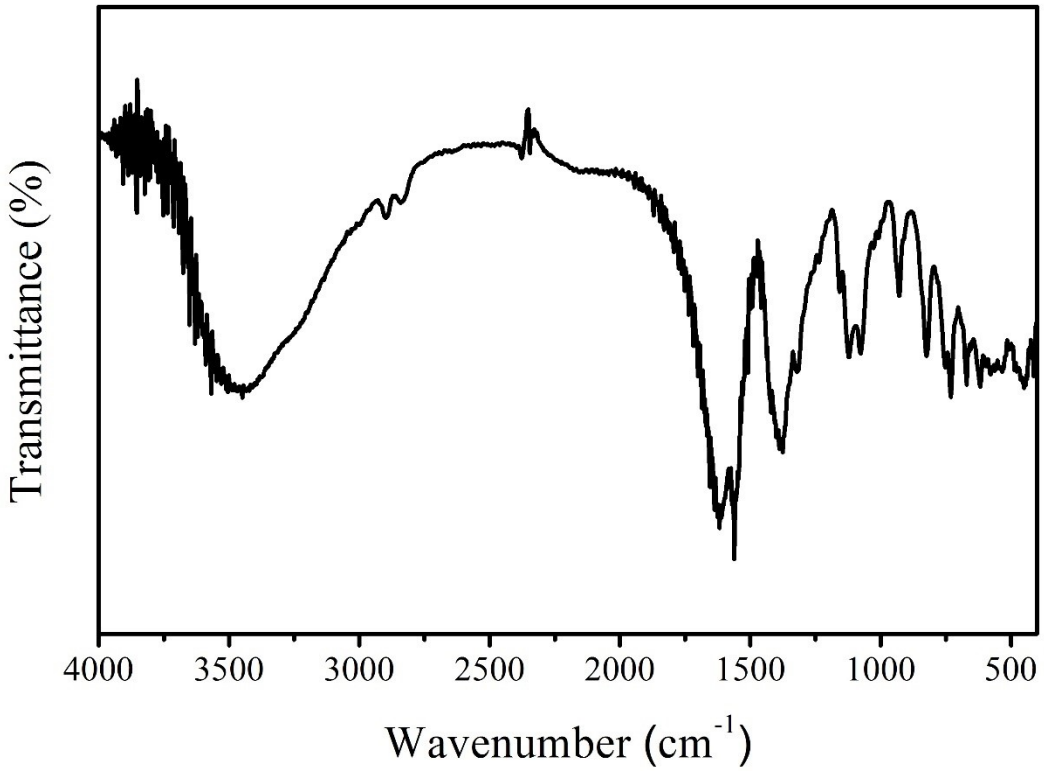

Fig. S26. IR spectrum of **5** (measured in KBr pellets).

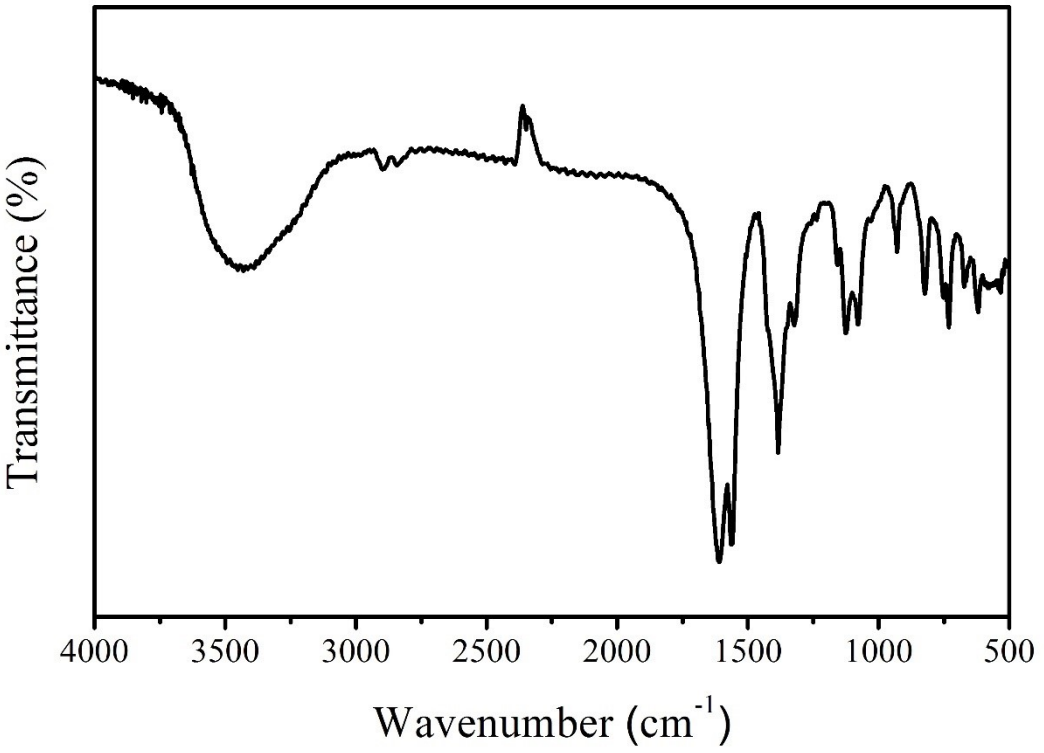

Fig. S27. IR spectrum of **7** (measured in KBr pellets).

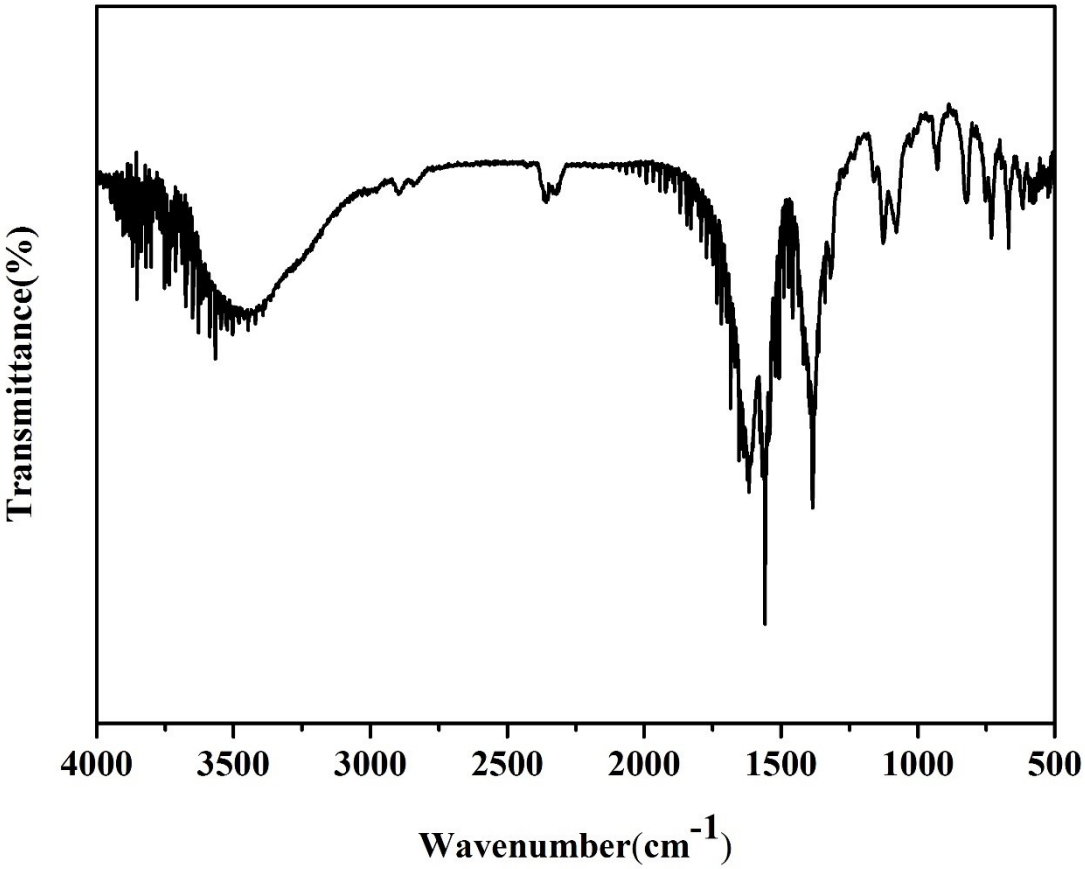

Fig. S28. IR spectrum of **2** (measured in KBr pellets).

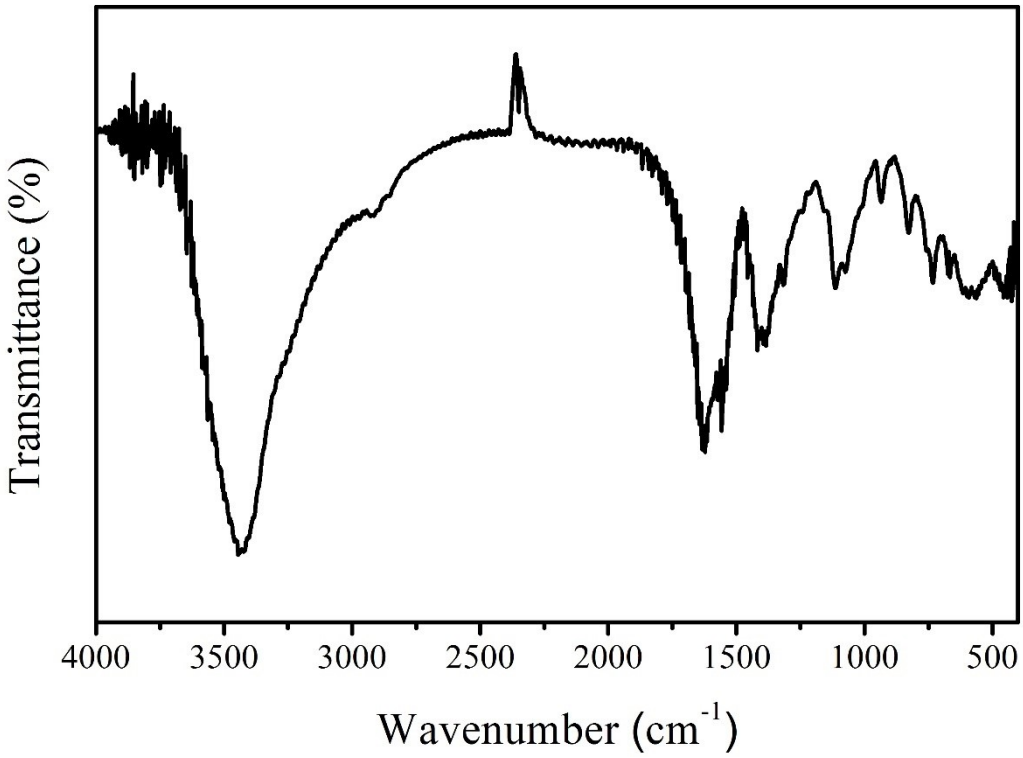

Fig. S29. IR spectrum of **4** (measured in KBr pellets).

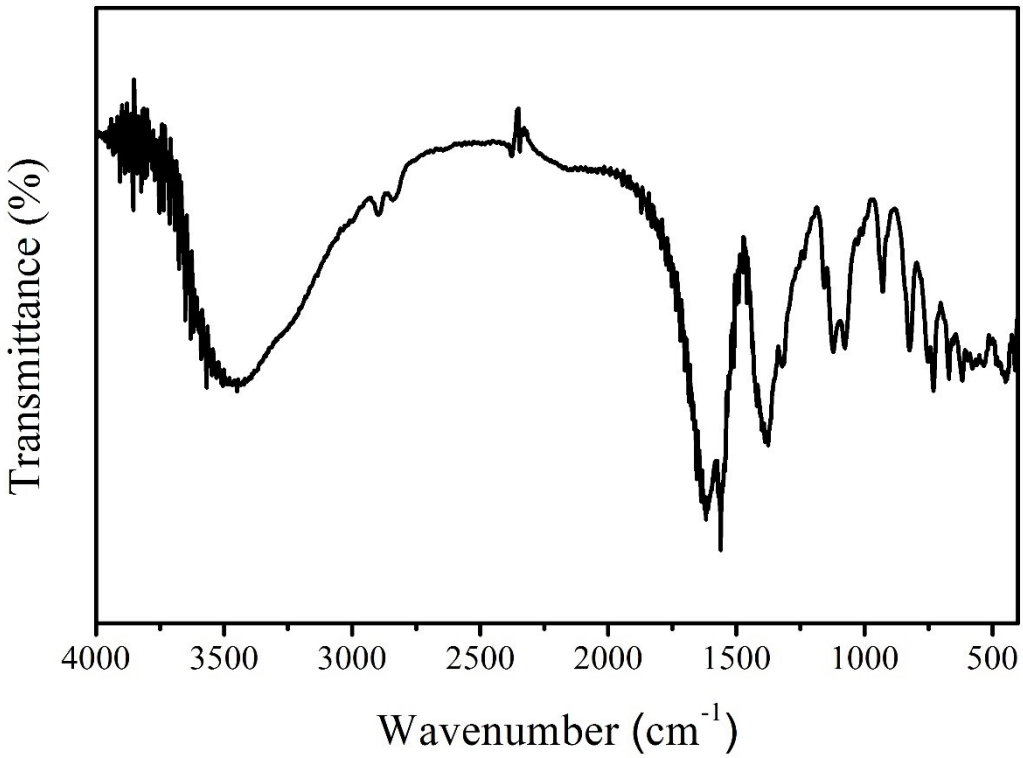

Fig. S30. IR spectrum of **6** (measured in KBr pellets).

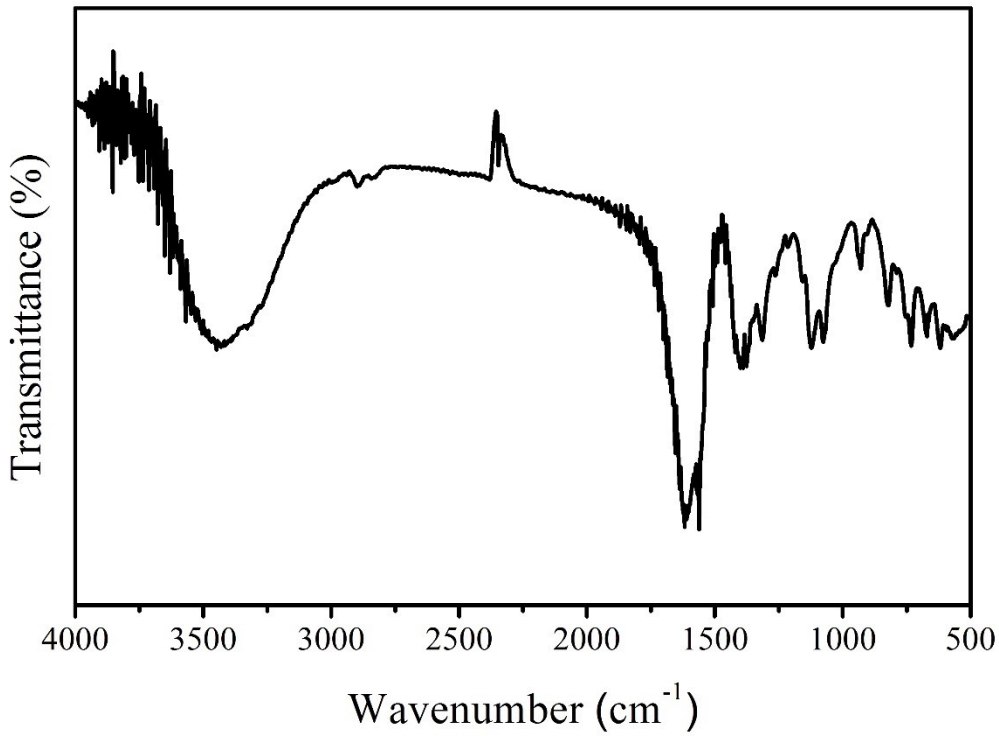

Fig. S31. IR spectrum of **8** (measured in KBr pellets).

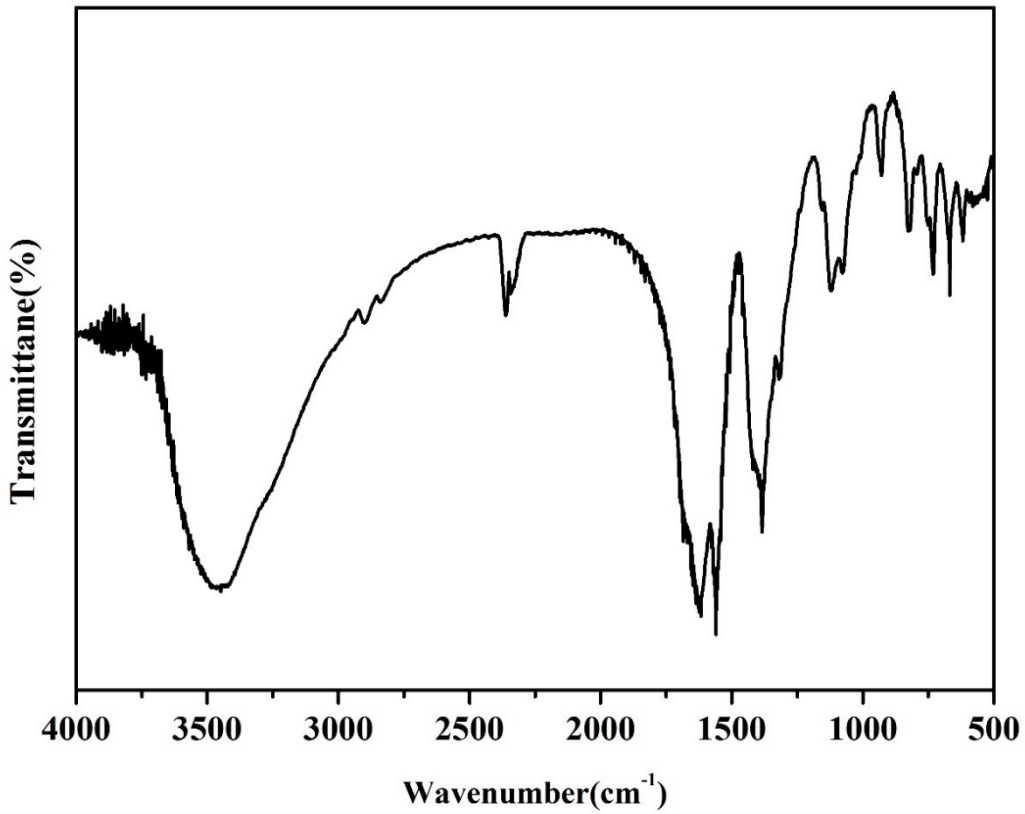

Fig. S32. IR spectrum of **9** (measured in KBr pellets).

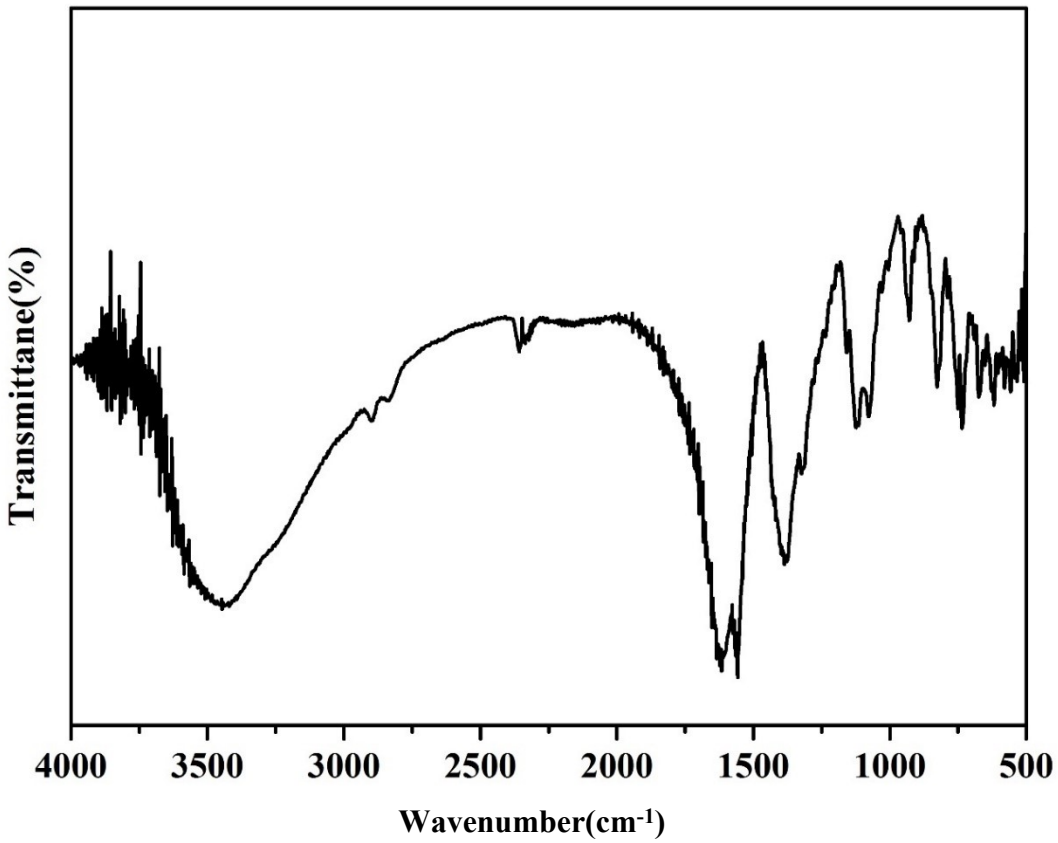

Fig. S33. IR spectrum of **10** (measured in KBr pellets).

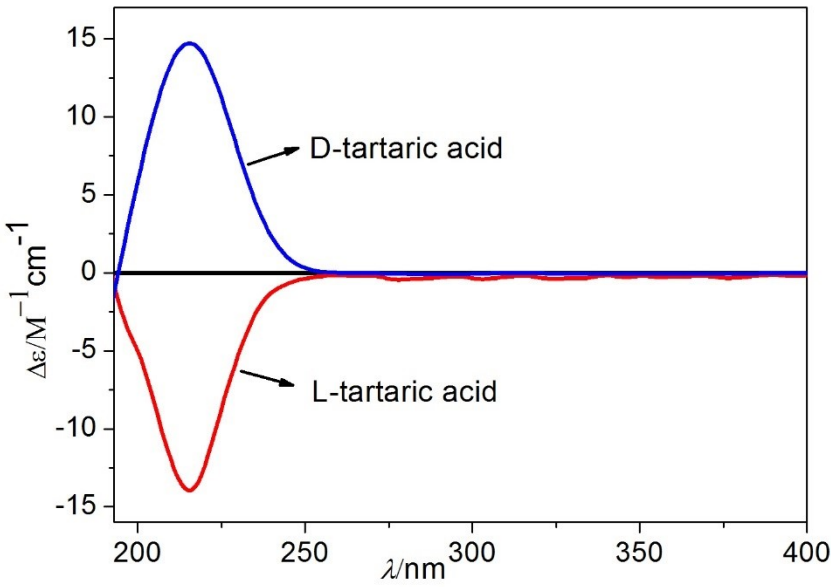

Fig. S34. CD spectra of L-(+)- and of D-(-)-tartaric acid in H_2O.

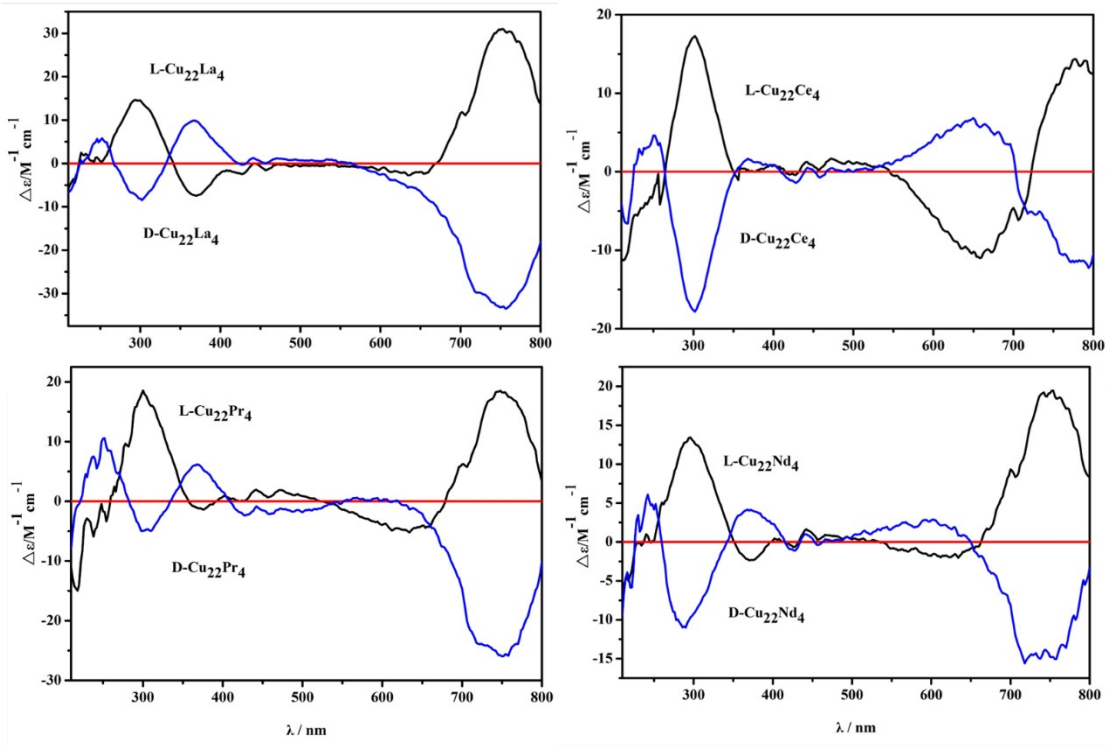

Fig. S35. CD spectra in the solid state: a) **1** (black), **2** (red); b) **3** (black), **4** (red); c) **5** (black), **6** (red) and d) **7** (black), **8** (red).

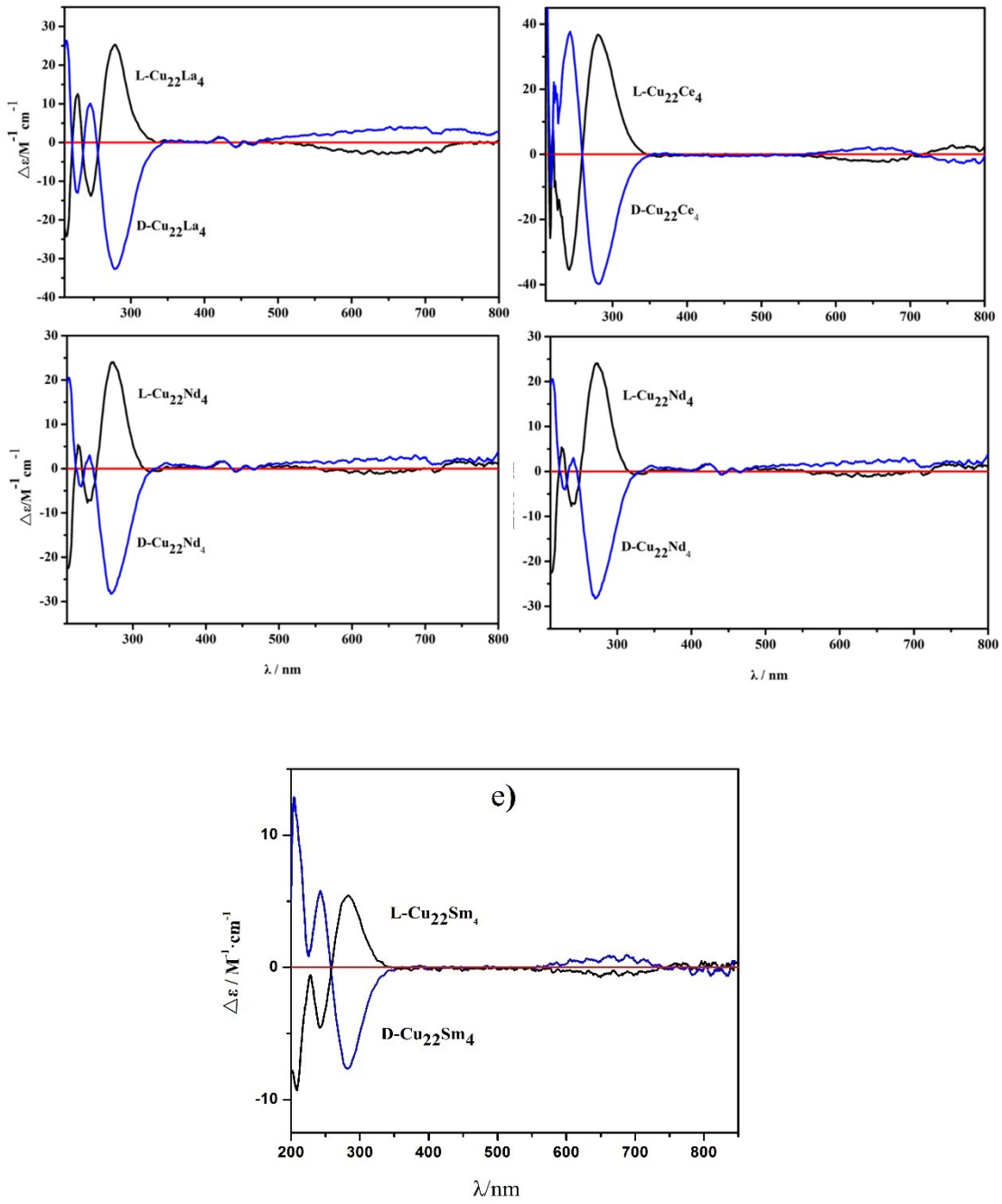

Fig. S36. CD spectra in the solution: a) **1** (black), **2** (blue); b) **3** (black), **4** (blue); c) **5** (black), **6** (blue) and d) **7** (black), **8** (blue), **9** (black), **10** (blue).

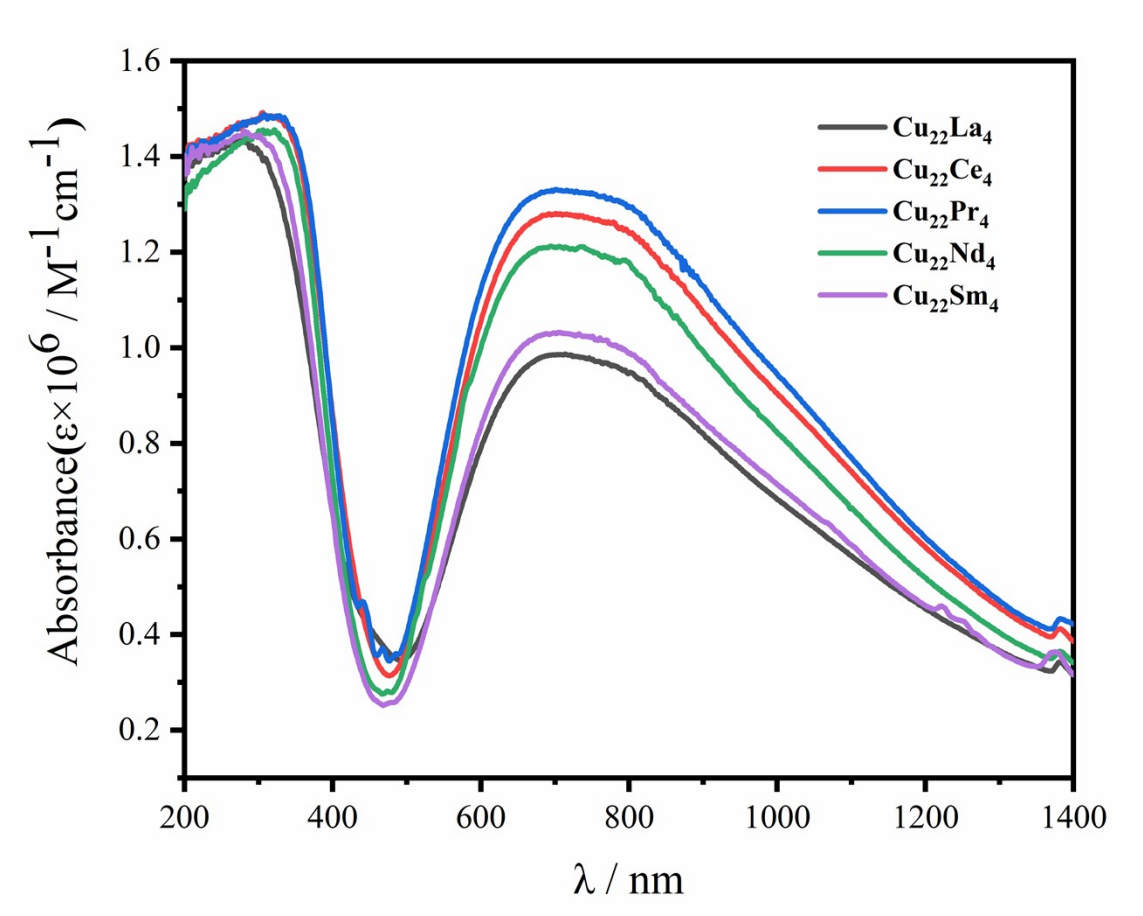

Fig. S37. The solid UV-VIS-NIR of **1**, **3**, **5**, **7**, **9**

Section S4: OA Z-Scan test results

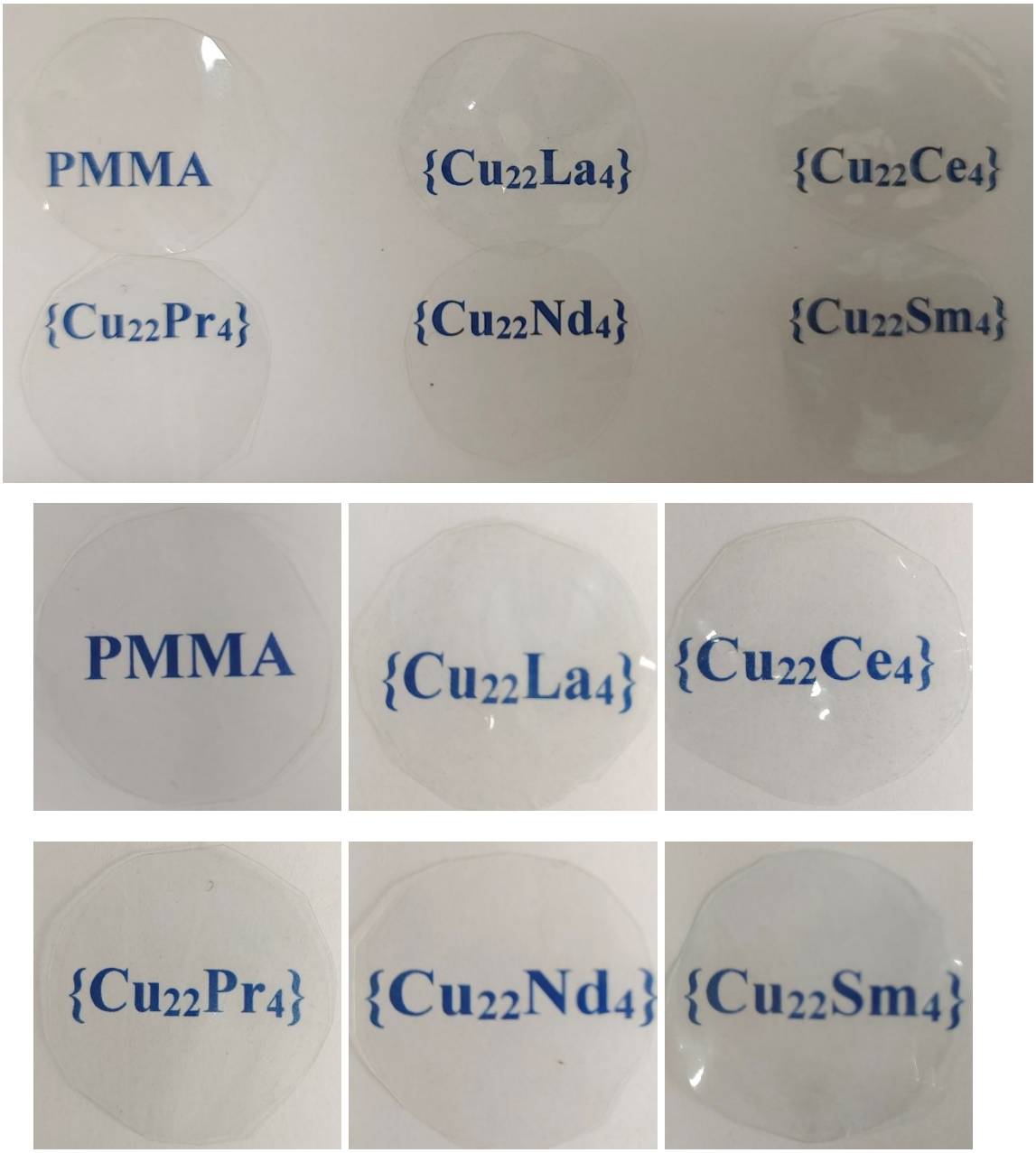

Fig. S38. Images of PMMA-based thin film and PMMA-based L-$Cu_{22}Ln_4$ (Ln= La, Ce, Pr, Nd, and Sm) thin films with same thickness

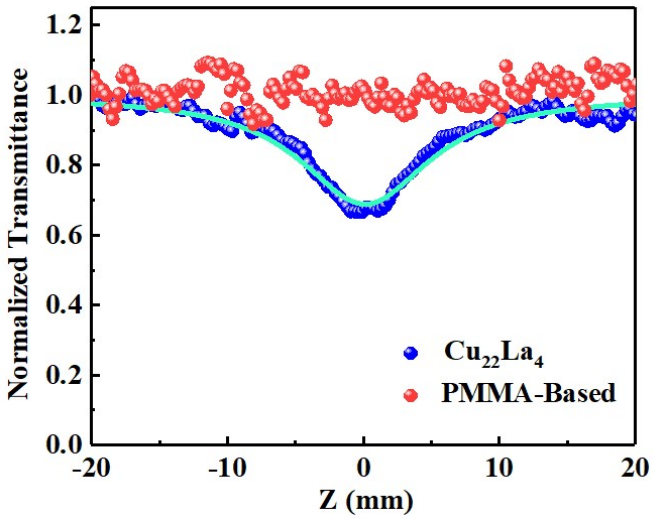

Fig. S39. The open-aperture Z-scan results at 800 nm for two thin films

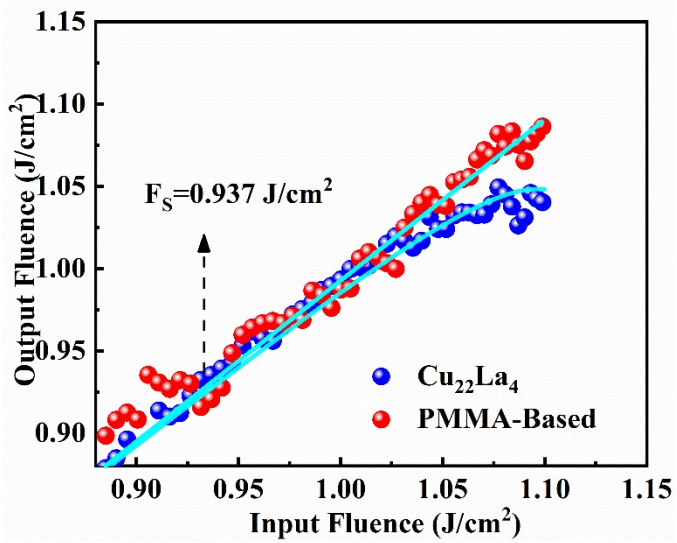

Fig. S40. the curves of output fluence versus input fluence for two thin films

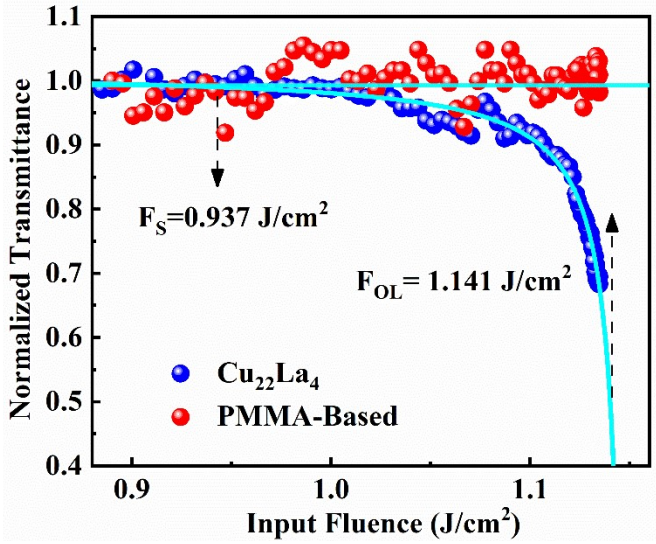

Fig. S41. variation in the normalized transmittance as a function of input intensity for two thin films

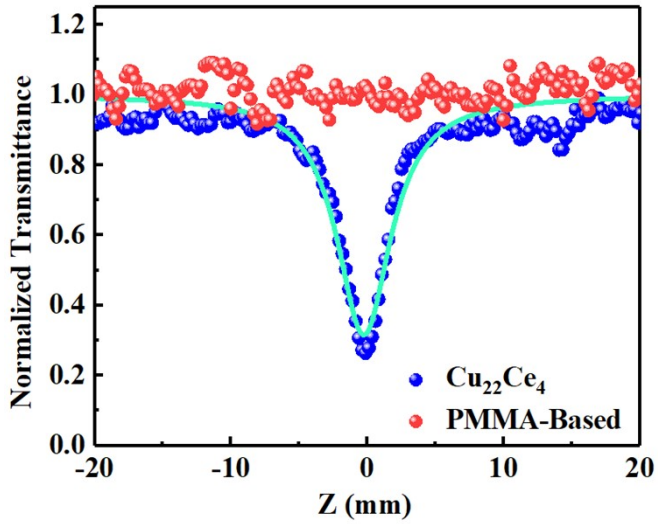

Fig. S42. The open-aperture Z-scan results at 800 nm for two thin films

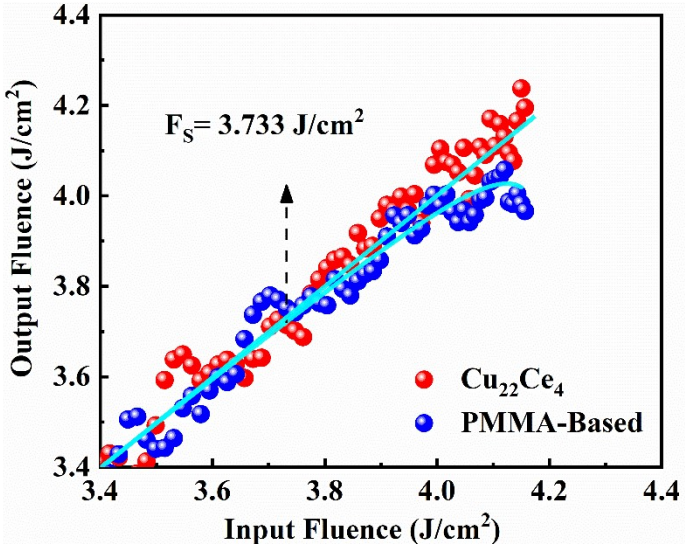

Fig. S43. the curves of output fluence versus input fluence for two thin films

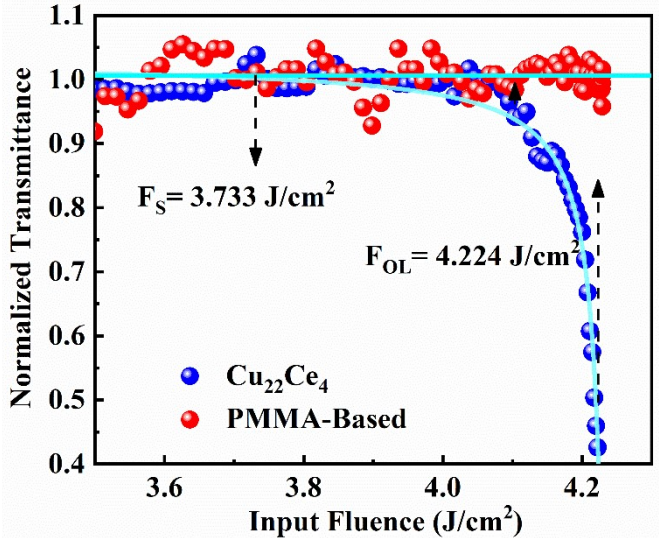

Fig. S44. variation in the normalized transmittance as a function of input intensity for two thin films

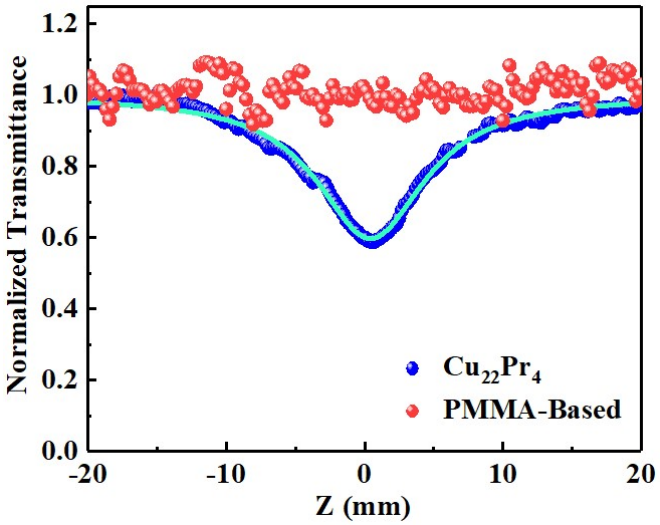

Fig. S45. The open-aperture Z-scan results at 800 nm for two thin films

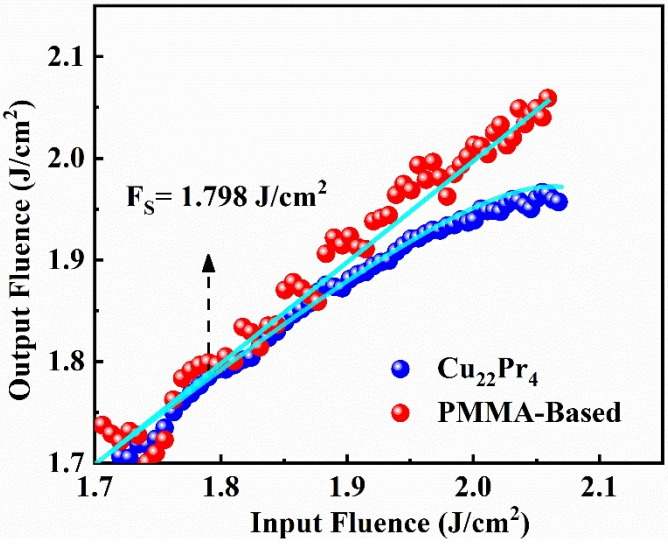

Fig. S46. the curves of output fluence versus input fluence for two thin films

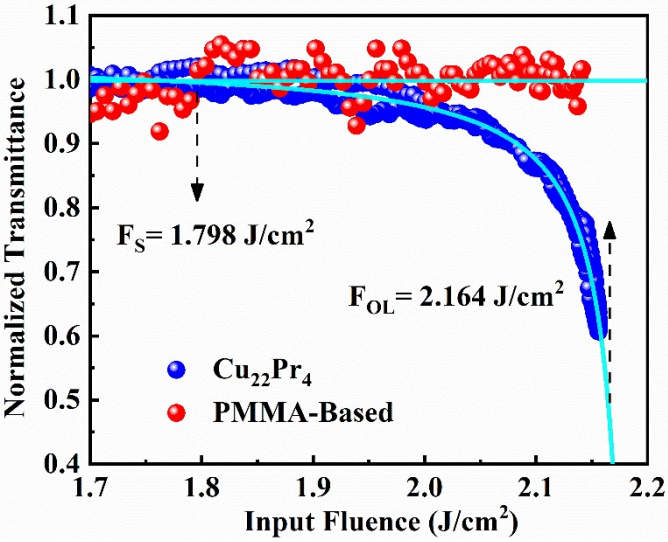

Fig. S47. variation in the normalized transmittance as a function of input intensity for two thin films

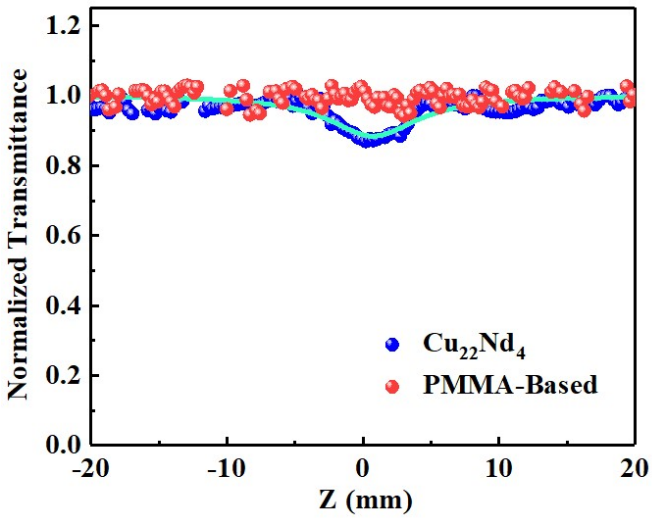

Fig. S48. The open-aperture Z-scan results at 800 nm for two thin films

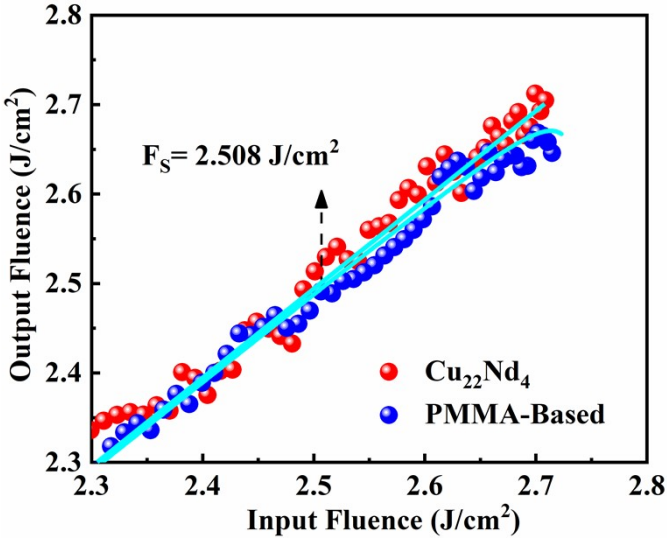

Fig. S49. the curves of output fluence versus input fluence for two thin films

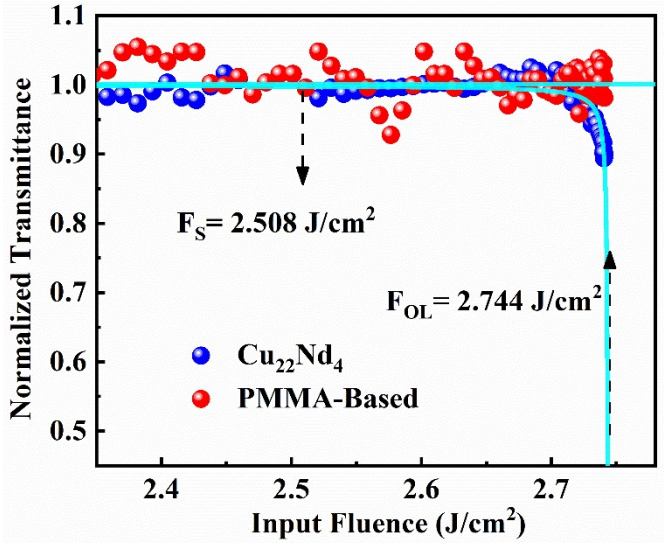

Fig. S50. variation in the normalized transmittance as a function of input intensity for two thin films

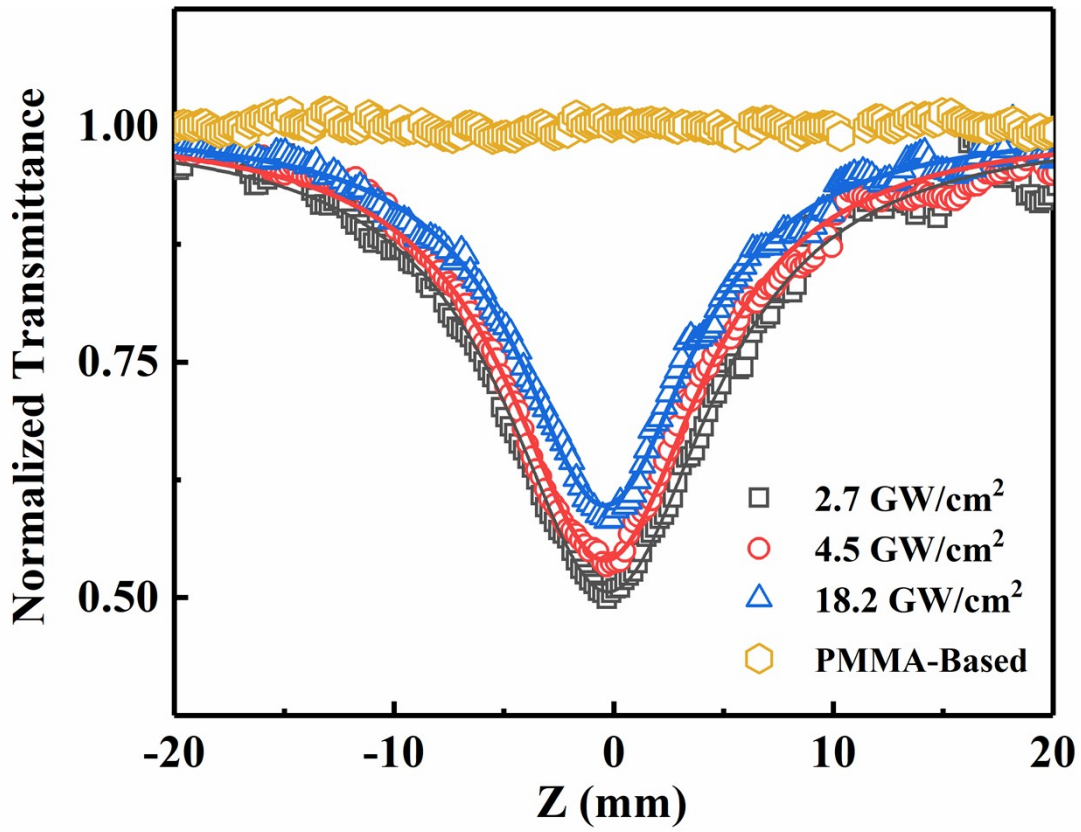

Fig S51. PMMA-Based $Cu_{22}Pr_4$ exhibits RSA characteristics at 2.7, 4.5, 18.3 GW/cm^2 light intensity irradiance at same position. The PMMA substrate under 18.2 GW/cm^2 laser excitation.

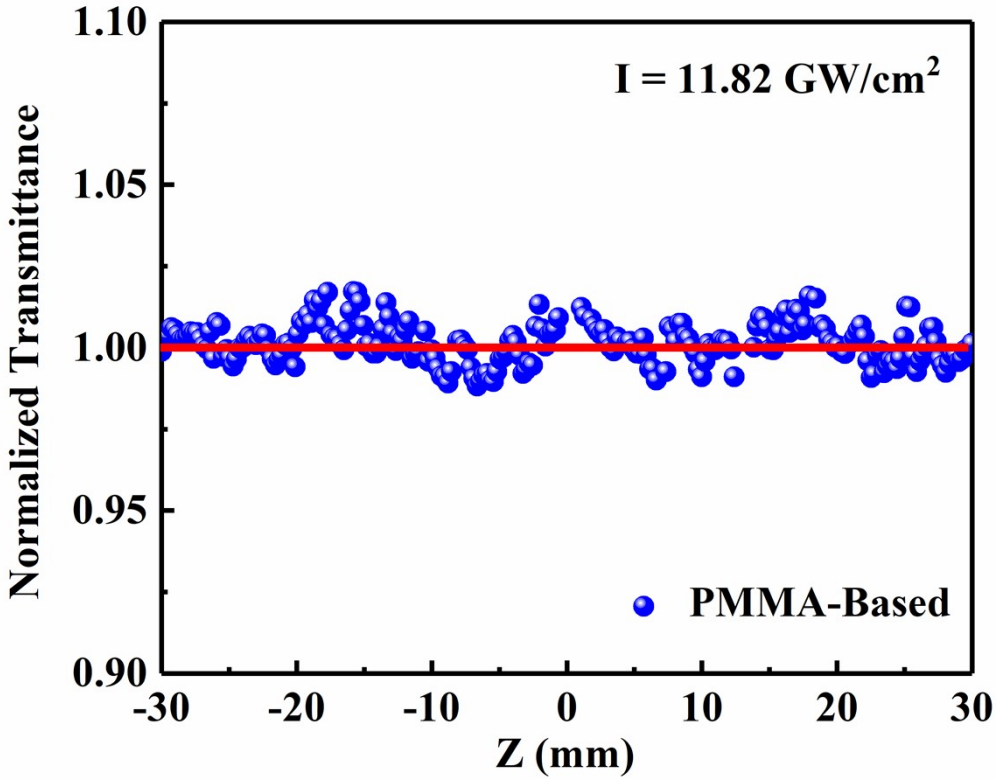

Fig S52. The PMMA substrate has no nonlinear absorption (i.e. flat response with Z) under 18.2 GW/cm^2 laser excitation.

Table S2. the fs Z-scan experiments at excitation wavelengths of 800 nm. (β: the third-order nonlinear absorption coefficient.)

Compound	Z-scan Experiments	Input intensity (W/cm^2)	β (m/W)	Nonlinear Absorption Type	Ref
PMMA-Based $Cu_{22}Sm_4$ thin film	pulse width:35 fs, repetition rate: 1 kHz	2.27×10^{12}	1.34×10^{-8}	RSA	This work
PMMA-Based $Cu_{22}La_4$ thin film		3.27×10^{11}	3.36×10^{-8}		
PMMA-Based $Cu_{22}Ce_4$ thin film		4.55×10^{12}	5.32×10^{-9}		
PMMA-Based $Cu_{22}Pr_4$ thin film		1.18×10^{12}	1.20×10^{-8}		
PMMA-Based $Cu_{22}Nd_4$ thin film		1.91×10^{12}	2.15×10^{-9}		
ErFeO3 film	pulse width: 50 fs, repetition rate: 1 kHz	4.00×10^{11}	2.38×10^{-10}	RSA	3
		4.50×10^{11}	2.50×10^{-10}		
		5.51×10^{10}	1.04×10^{-9}		
		1.95×10^{10}	2.75×10^{-9}		
$CsPbBr_3$ solution (3.4×10^{-5} mol/L)	pulse width: 100 fs, repetition rate: 1 kHz	2.00×10^{10}	9.70×10^{-13}	RSA	4
terpyridine-based zinc(II) complexes in DMSO	pulse width: 140 fs, repetition rate: 10 Hz	/	4.30×10^{-14}	RSA	5
Silver Nanoparticles Embedded Borate Glasses	pulse width: 150 fs, repetition rate: 80 MHz	/	1.28×10^{-11}	RSA	6
composite film of complex and PMMA	pulse width: 90 fs, repetition rate: 92 MHz	8.00×10^{9}	-2.3×10^{-10}	SA	7
silver nanoparticles embedded bismuthate glasses	pulse width: 200 fs, repetition rate: 76 MHz	1.42×10^{9}	8.12×10^{-12}	RSA	8
$90GeS_2$-$10In_2S_3$	pulse width: 130 fs, repetition rate: 76 MHz	5.20×10^{8}	1.20×10^{-11}	RSA	9

References

1. L. Huang, C. Zheng, Q. Guo, D. Huang, X. Wu and L. Chen, *Optical Materials.*, 2018, **76**, 335-343.
2. M. Sheik-Bahae, A. A. Said, T. H. Wei, D. J. Hagan and E. W. V. Stryland, *IEEE J Quantum Electron.*, 1990, **26**, 760-769.
3. A. Gaur, M. A. Mohiddon and V. R. Soma, *J. Appl. Phys.*, 2020, **127**, 173104
4. Y. Wang, X. Li, X. Zhao, L. Xiao, H. Zeng and H. Sun, *Nano Lett.*, 2016, **16**, 448-453.
5. Y. Tang, M. Kong, X. Tian, J. Wang, Q. Xie, A. Wang, Q. Zhang, H. Zhou, J. Wu and Y. Tian, *J. Mater. Chem. B.*, 2017, **5**, 6348-6355.
6. K. Keshavamurthy, B. N. Swetha, K. N. Sathish, A. G. Pramod, I. Kebaili, M. I. Sayyed, S. Itigi, P. Ramesh, V. Hegde, N. Linga Murthy, S. Venugopal Rao and G. Jagannath, *Infrared Phys Technol.*, 2021, **119**, 103959.
7. B. J. Rudresha, B. R. Bhat, D. Ramakrishna, J. K. Anthony, H. W. Lee and F. Rotermund, *Opt Laser Technol.*, 2012, **44**, 1180-1183.
8. F. Chen, J. Cheng, S. Dai and Q. Nie, *J Non Cryst Solids.*, 2013, **377**, 151-154.
9. Y. Yang, O. Ba, S. Dai, F. Chen and G. Boudebs, *J Non Cryst Solids.*, 2021, **554**, 120581.